Space Sci Rev (2009) 144: 351–381
DOI 10.1007/s11214-008-9461-x

Magnetic Flux Emergence, Activity, Eruptions and Magnetic Clouds: Following Magnetic Field from the Sun to the Heliosphere

L. van Driel-Gesztelyi · J.L. Culhane

Received: 23 September 2008 / Accepted: 31 October 2008 / Published online: 29 November 2008

Abstract We present an overview of how the principal physical properties of magnetic flux which emerges from the toroidal fields in the tachocline through the turbulent convection zone to the solar surface are linked to solar activity events, emphasizing the effects of magnetic field evolution and interaction with other magnetic structures on the latter. We compare the results of different approaches using various magnetic observables to evaluate the probability of flare and coronal mass ejection (CME) activity and forecast eruptive activity on the short term (i.e. days). Then, after a brief overview of the observed properties of CMEs and their theoretical models, we discuss the ejecta properties and describe some typical magnetic and composition characteristics of magnetic clouds (MCs) and interplanetary CMEs (ICMEs). We review some individual examples to clarify the link between eruptions from the Sun and the properties of the resulting ejecta. The importance of a synthetic approach to solar and interplanetary magnetic fields and activity is emphasized.

Keywords Magnetic flux emergence · Magnetic observables · Flare · Coronal mass ejection · Magnetic cloud · ICME

1 Introduction

Day after day enormous amounts of magnetic flux emerge on the Sun: $\Phi \leq 10^{24}$ Mx not accounting for the hidden turbulent magnetic flux (Lites et al. 2007). The observable flux appears on different scales ($10^{18} \leq \Phi \leq 10^{23}$ Mx) forming active regions (ARs), ephemeral

L. van Driel-Gesztelyi (✉) · J.L. Culhane
University College London, Mullard Space Science Laboratory, Holmbury St. Mary, Dorking, Surrey, RH5 6NT, UK
e-mail: Lidia.vanDriel@obspm.fr

L. van Driel-Gesztelyi
Observatoire de Paris, LESIA, FRE 2461(CNRS), 92195 Meudon Principal Cedex, France

L. van Driel-Gesztelyi
Konkoly Observatory of Hungarian Academy of Sciences, Budapest, Hungary

regions (ERs), and on as small a scale as the inter-network field (INF). The frequency distribution of flux emergence over its scale spectrum is smooth and continuous spanning almost five orders of magnitude in flux and eight orders of magnitude in frequency (10^4–10^{-4} day^{-1}; Hagenaar et al. 2003; Meunier 2003). The daily magnetic flux emergence rate is highest on the smallest scale, dominating the flux budget at any given moment. However, the overturn time of small-scale flux is only a few minutes (Lites et al. 1996), therefore the long-surviving large-scale flux determines the magnetic properties of the Sun. Furthermore, it is the large-scale flux, which is responsible for the most energetic activity events. Thus in this review we concentrate on the magnetic characteristics of large-scale flux emergence forming ARs.

Large-scale flux emergence reveals physical processes related to magnetic field generation and transport in the sub-photospheric layers. Emergent flux carries clues about the (i) characteristics of dynamo, but also about (ii) conditions in the convection zone with which it interacted during its ascent to the surface and in which the subsurface part of the flux-tube is still embedded. Furthermore, magnetic characteristics of ARs (iii) determine their eruptive activity leading to flares and coronal mass ejections, where the latter expel huge amount of plasma and magnetic field into interplanetary space. Magnetic flux tubes observed *in-situ* close to the Earth and beyond have a direct continuity to their solar source: they represent flux, which has been amplified by the global dynamo at the bottom of the convection zone (Parker 1993 and for a recent review see Gilman 2005), became buoyant, emerged to the surface and was eventually launched by an MHD instability into the interplanetary space. Keeping this continuity in mind we review the principal characteristics of emerging flux (Sect. 2) and active region decay (Sect. 3) focussing on how much we know about the link between these characteristics and the occurrence of solar eruptive events (i.e. our ability to predict flares and coronal mass ejections; Sect. 4). Then, after a brief overview of CME models (Sect. 5), and ICME and magnetic cloud characteristics (Sect. 6) we illustrate by describing a few case studies how well we presently understand the link between solar eruptions and their interplanetary consequences (Sect. 7). We conclude in Sect. 8, emphasizing the importance of a synthetic view.

2 Flux Emergence

2.1 The Three Main Rules of Magnetic Flux Emergence

Since helioseismology is presently unable to 'detect' magnetic field in the solar interior deeper than a few Mm, dynamo models must rely on boundary conditions provided by direct observations of the magnetic fields in the solar atmosphere. The three main observationally established rules of solar activity related to the orientation and emergence patterns of sunspot groups (bipoles) during the 11/22-year solar cycle, namely Hale's law (Hale and Nicholson 1925), the butterfly diagram (or Spörer's law; Carrington 1858) and Joy's law (Hale et al. 1919), are the pillars of all successful dynamo models.

Hale's law states that bipolar active regions (ARs) that are aligned roughly in the east-west direction, on opposite hemispheres have opposite leading magnetic polarities (leading in the sense of solar rotation). The magnetic polarities are alternating between successive sunspot cycles. Spörer's law (i.e. the butterfly diagram) expresses that the latitudes of flux emergence show a dependence on the solar cycle. When the cycle begins ARs first emerge at high latitudes then tend to emerge at progressively lower latitudes as the cycle progresses. Joy's law recognizes that there is a systematic deviation from the east-west alignment of bipolar ARs with the leading spots being closer to the equator on both solar hemispheres.

These basic rules were recognized not long after (or even before!) the discovery of solar magnetism a hundred years ago (Hale 1908).

2.2 Additional Characteristics: Asymmetries and Tilt

More recently, some additional physical characteristics of emerging flux were recognized providing further clues to the flux generation by the dynamo and flux transport in the convection zone, as well as for understanding eruptive activity.

The asymmetries in bipolar ARs, namely that (i) the leading sunspots are larger and longer-lived than following spots and (ii) in the divergent motions during emergence the leading sunspots move much faster westward than the following spots eastward, were explained as being due to a systematic eastward tilt of emerging flux tubes (van Driel-Gesztelyi and Petrovay 1990). MHD simulations in the thin flux tube approximation showed that buoyant rising flux tubes become inclined to the vertical while emerging through the convection zone due to the conservation of the angular momentum (Moreno-Insertis et al. 1994; Caligari et al. 1995; Abbett et al. 2001). Conservation of angular momentum induces an eastward (retrograde) plasma flow in the flux tube decreasing the plasma pressure in the leading, while increasing it in the following leg (Fan et al. 1993). Pressure equilibrium requires an inverse change in magnetic pressure leading to an asymmetry in stability between the leading and following spots in ARs. However recent 3-D spherical shell inelastic MHD simulations of the buoyant rise of magnetic flux tubes through the convection zone by Fan (2008) presented a very different picture on the origin of these asymmetries. She showed that due to asymmetric stretching of the rising flux tube by the Coriolis force, a field strength asymmetry develops with the field strength in the leading leg being stronger than the field in the following leg, which results in larger and more stable leading spots. Another consequence is that the leading legs of Ω-loops become more buoyant, producing an asymmetry in the Ω-loops' shape which is *opposite* to that of the simulations in the thin flux tube approximation. Therefore the asymmetry in the divergent motions between the leading and following spots of emerging bipoles cannot be explained by the sub-photospheric shape of the emerging Ω-loop as proposed by van Driel-Gesztelyi and Petrovay (1990). Instead, based on the results of these 3-D simulations, we suggest that the asymmetry in sunspot proper motions is caused by the faster rise of the leading than that of the following leg of the Ω-loop.

The tilt of bipolar ARs relative to the E–W direction, which increases with latitude and is described by Joy's law was shown to be caused by the Coriolis force (Schmidt 1968; Fisher et al. 1995). However, tilt can also be caused by large-scale vortices in the convective zone deforming the rising flux tube (López-Fuentes et al., 2000, 2003). The effect of turbulent buffeting of rising flux tubes is well demonstrated by departures from Joy's law which increase with decreasing flux content of the emerging bipoles (Harvey 1993; Longcope and Fisher 1996). Such turbulent perturbations, if created in the topmost layer of the convection zone, should relax rapidly (Longcope and Choudhuri 2002) turning the flux tube to conform with Joy's law.

2.3 Inherent Twist and Its Implications

The potentially widest-ranging impact came from the recognition, that emerging flux is inherently twisted. Leka et al. (1996) were the first to provide observational evidence for flux emergence in a non-potential state, inspiring research contributing to a revival of interest in helicity. Non-potential magnetic flux emergence has a very important relevance for solar activity: such emerging flux carries free magnetic energy 'ready' to be released. Photospheric

shearing motions, which have been long thought to be the generators of magnetic stresses, may simply reflect the emergence of a twisted structure as successive cross-sections of a helical structure can easily be mis-interpreted as shearing flows Démoulin and Berger (2003). Nevertheless, plasma flows do exist on the Sun, therefore their effects on emerged fields should not be dismissed. Rather, twisted flux emergence and large-scale flows are both responsible for the free energy level of the magnetic field structures we see on the Sun.

Prior to the observational evidence by Leka et al. (1996) theoretical arguments have been raised in favour of non-potential flux emergence from considerations of the energy available for flaring (McClymont and Fisher 1989; Melrose 1992). Furthermore, Schüssler (1979) and later Longcope et al. (1996), through MHD simulations, showed that non-twisted flux cannot even make it through the convection zone due to a strong tendency for fragmentation. However, the flux tube cannot be fragmented by eddies forming in its wake but can remain coherent if it is sufficiently twisted (Moreno-Insertis and Emonet 1996). Many other simulations have been carried out since, verifying this result while probing deeper into details of inherent twist in emerging flux tubes (see e.g. Murray and Hood 2008). These simulation results imply that inherent twist is a general property of flux emergence on the Sun, i.e. that all the large-scale flux that has crossed the convection zone must be twisted and must therefore possess magnetic helicity.

Magnetic helicity is a quantitative, mathematical measure of the chiral properties of magnetic structures. Chirality patterns discovered in active regions, coronal loops, filaments, coronal arcades and interplanetary magnetic clouds (Pevtsov and Balasubramaniam 2003, and references therein) indicate that the Sun preferentially exhibits left-handed features in its northern hemisphere and right-handed features in the south. A right-handed twist and a clockwise rotation of the loops when viewed from above implies positive helicity, and *vice versa* for negative helicity. Exceptions to these helicity rules occur in most categories of solar activity at a significant level (20–35%). Nevertheless, the Sun's preference for features adhering to these rules is suggestive of underlying mechanisms related to the working of the dynamo and differential rotation that are, evidently, global in scope.

However, it must be noted that observations indicate a relatively low level of twist in emerging flux regions as deduced from both current helicity (Longcope et al. 1999) and photospheric magnetic helicity flux measurements (Démoulin and Pariat 2008, and references therein), the latter being compatible with a 0.01–0.2 end-to-end twist of field lines between their photospheric footpoints in emergent flux ropes.

Recent 3-D spherical shell inelastic MHD simulations of the buoyant rise of magnetic flux tubes through the convection zone by Fan (2008), cited above, also, indicate that the initial level of twist must be lower than indicated by previous simulations. Fan's 3-D simulations show that for tubes with the twist rate that is necessary for a cohesive rise, the twist-induced tilt (deformation of the flux tube at its apex) dominates that caused by the Coriolis force, and furthermore, the twist-induced tilt is of the wrong direction (opposite to the observational Joy's law) if the twist is left-handed (right-handed) in the northern (southern) hemisphere, following the observed hemispheric preference of the sign of the active region twist. In order for the emerging tube to show the correct tilt direction (consistent with observations), the initial twist rate of the flux tube needs to be less than half of that needed for a cohesive rise. Under such conditions, however, severe flux loss was found during the rise, with less than 50% of the initial flux remaining in the Ω-loop by the time it reaches the surface.

The emergence of even a mildly twisted flux rope has its caveats as dense plasma accumulating in its concave-up parts located below the axis of the flux rope practically anchor its U-loop sections in and below the photosphere. Furthermore, due to fast changes in physical conditions, the flux rope has great difficulties in crossing the photosphere (e.g., Magara

2004; Manchester et al. 2004) leading to its fragmentation. Emergence of a flux rope therefore must involve many episodes of magnetic reconnection to succeed (Pariat et al. 2004). Nevertheless, characteristic magnetic polarity distribution patterns in longitudinal magnetic maps of emerging flux regions dubbed "magnetic tongues", first identified and interpreted as the signature of the azimuthal field component in an emerging flux rope by López Fuentes et al. (2000) do indicate that there is an overall organization in the emerging flux tube, which is compatible with a global twist. These "magnetic tongues" are present as long as the top part of the twisted flux rope crosses the photosphere and they can be used as a proxy for determination of the helicity sign of an active region (Green et al. 2007).

2.4 Magnetic Helicity

Magnetic helicity quantifies how the magnetic field is sheared and twisted compared to its lowest-energy state; the potential (or current-free) field. However, unlike other physical quantities of magnetic stress (e.g. shear) magnetic helicity can be precisely *quantified* in a given magnetic configuration and possesses the unique property of being almost completely conserved even in resistive MHD on time-scales involved in solar activity events and during magnetic reconnection (Berger 1984). Helicity generation is a natural product of dynamo processes and potentially saturates the dynamo (α-effect quenching); for a recent review, see Brandenburg and Subramanian (2005).

Magnetic helicity is the volume integral of the product of magnetic vector potential $\mathbf{A}$ and magnetic field $\mathbf{B}$ ($\mathbf{B} = \nabla \times \mathbf{A}$). Since $\mathbf{A}$ is not a measurable quantity and has a gauge freedom, magnetic helicity remained a theoretical concept for decades. It was only very recently, that theoretical developments allowed observational applications, making helicity studies the most dynamically developing field of solar physics. As a more easily computable quantity, current helicity ($H = \int \mathbf{B} \cdot \mathbf{j}\, d^3x$, with $\mu_0 \mathbf{j} = \nabla \times \mathbf{B}$) was widely used. Current helicity measures the curl of $\mathbf{B}$ along the magnetic field quantifying local twist. Magnetic and current helicity usually have the same sign, but they also have basic differences, e.g. current helicity is not a conserved MHD quantity. Observational studies of magnetic helicity and current helicity both helped to quantify twisted flux emergence and enhance our understanding of the build-up of eruptive activity on the Sun.

Based on tracking photospheric flows, methods have been developed to measure the magnetic helicity flux (or rate) through the photosphere ranging from the first estimation by Wang (1996) and the first measurements by Chae (2001) to more recent developments involving a new method to measure helicity flux density, or helicity flux through the photosphere per unit surface (Pariat et al. 2005, 2006). The bulk of the helicity is clearly injected during the main phase of flux emergence with at first (for about two days) a lower, followed by a higher rate, increasing in tandem with the magnetic flux (Jeong and Chae 2007; Tian and Alexander 2008). The temporal profile of magnetic helicity flux is indicative of helicity brought up by a twisted flux tube (c.f. Cheung et al. 2005; Chae et al. 2004; Pariat et al. 2005, and for an assessment see a review by Démoulin 2007). Coronal helicity content of ARs can be computed from magnetic extrapolations (e.g. Démoulin et al. 2002; Green et al. 2002a; Mandrini et al. 2005). The coronal helicity content of ARs, like that of emerging flux, appears to be modest, being equivalent to that of a twisted flux tube having 0.2 turn with $\mathbf{H}_{\max}(\mathrm{AR}) \approx 0.2\text{–}0.01\Phi^2$, where Φ is the total magnetic flux of the AR (Démoulin 2007; Démoulin and Pariat 2008). From coronal helicity estimates before and after a CME, the loss of magnetic helicity from an AR was assessed (Bleybel et al. 2002). Methods for helicity calculations in magnetic clouds (MCs) have been developed and compared with the decrease of helicity in the CME source region, the two being in satisfactory agreement (Mandrini et al. 2005; Luoni et al. 2005). For an insightful review on recent theoretical

and observational results on magnetic helicity in the Sun and the interplanetary space see Démoulin (2007).

The cycle-invariant relentless accumulation of helicity in the solar corona being brought up by emerging flux and generated by differential rotation combined with its well-conserved nature also poses a problem. Though some helicity can be canceled between the two hemispheres through magnetic reconnection of opposite helicity structures (Pevtsov 2000), such reconnections involve only a small fraction of the flux present on the Sun, therefore this mechanism is probably insufficient to relieve the buildup. Rust (1994) and Low (1997) suggested that the Sun only avoids endless accumulation of helicity in the solar atmosphere by ejecting helicity via CMEs.

The well-conserved nature of magnetic helicity provides us with a quantitative measure to be traced and compared as buoyant magnetic flux travels from the tachocline through the convection zone, emerges through the photosphere to the corona and is ejected into interplanetary space during CME events reaching the vicinity of the Earth and beyond as a magnetic cloud or ICME (Démoulin 2008).

2.5 Nesting Tendency of Flux Emergence

Harvey and Zwaan (1993) found a 22-fold higher emergence rate within existing ARs than elsewhere. Furthermore, there is a tendency for ARs to emerge in the immediate vicinity of an existing AR, or at the site of a previous AR, forming 'activity nests', which may exist as long as 6–7 months (Brouwer and Zwaan 1990). The nested nature of flux emergence is very strong, nearly 50% of all emergent bipoles being part of an active nest or activity complex (Schrijver and Zwaan 2000). The recurrent nature of flux emergence ('active longitudes', first noted by Carrington in 1858), has been linked to longitudinal wave numbers of magnetic instabilities in a concentrated toroidal field (Gilman and Dikpati 2000) and more recently to shallow-water instability of differential rotation and toroidal field bands in the solar tachocline (Dikpati and Gilman 2005).

This nested nature is reflected in the formation of some of the large, magnetically complex ARs as several bipolar ARs emerge separated, but in close proximity and in close succession within a few days (Schrijver and Zwaan 2000). Magnetic complexity and activity level are closely linked, as we will discuss in Sect. 3.

3 Decay of Active Regions

Once all the flux has emerged, or possibly even before that (Wang et al. 1991), active regions start to decay. After sunspots reach maximum area partially through coalescence of smaller umbrae, spots start shrinking and breaking up. Vigorous moving magnetic feature (MMF) activity is seen around spots carrying flux away (Harvey and Harvey 1973; Hagenaar and Shine 2005; Sainz Dalda and Martínez-Pillet 2005; Ryutova and Hagenaar 2007). There is a notable asymmetry in the time spent by an active region in emergence and decay: emergence lasts for hours to days ($\leq$ 5 days; Harvey 1993), while the decay of spots may last from days to several weeks (e.g. Hathaway and Choudhary 2008) and even in some cases months (van Driel-Gesztelyi et al. 1999). Active regions, even after the disappearance of their spots, remain distinguishable from their magnetic environment for up to seven months while their magnetic flux in a magnetically undisturbed environment during solar minimum spreads over an ever-increasing area (Fig. 1b; see also van Driel-Gesztelyi 1998) forming large bipolar regions shaped by an interplay of convective flows and differential rotation,

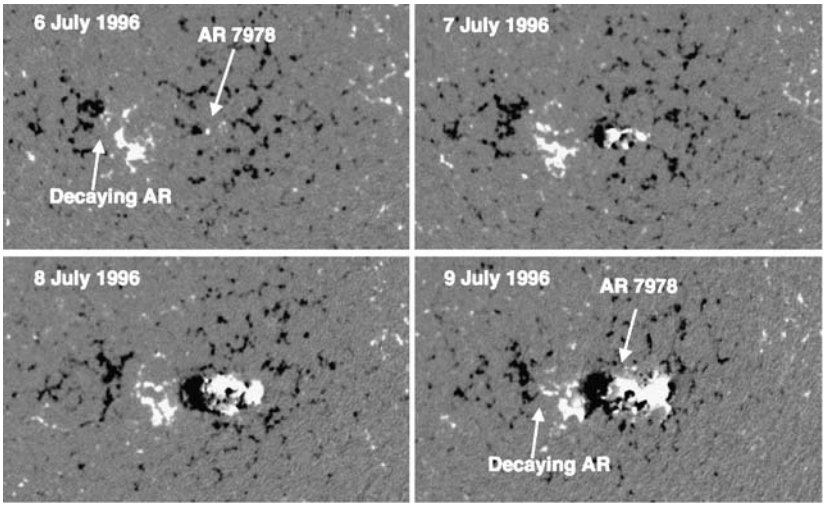

Fig. 1a SOHO/MDI magnetograms showing the emergence of NOAA AR 7978 in July 1996. The boundaries of the emerging bipole are outlined with a white contour. Note the decaying AR East to the growing AR 7978, which totally disappeared by the next rotation shown in Fig. 1b, presumably due to effective magnetic cancellation processes

which slowly become part of the 'background field'. During the decay process of active regions large-scale magnetic complexity is decreasing then disappears due to effective cancellation processes, unless the active region is part of an active nest and thus a place of repeated large-scale flux emergence. In the latter case, however, the evolution of the individual bipoles can be significantly shortened by magnetic cancellation. While the decay phase is marked by a decrease of magnetic flux density accompanied by a decrease of all plasma parameters (temperature, emission measure, pressure; van Driel-Gesztelyi et al. 2003) there is a remarkable growing feature in the AR. Filaments, which are absent, or if present, are short and variable when the AR is young, become stable and can reach a length of 10^5 km or more, becoming increasingly parallel to the equator. Though flare activity is fast disappearing with the decrease of magnetic flux density, coronal mass ejections may well occur during the decay stage due to the repeated eruption of the long filament.

3.1 The Effect of Magnetic Evolution on Activity

An exceptional opportunity for observing active region emergence and decay as well as the accompanying flare and CME activity arose during the previous solar minimum, when solar activity was dominated by a single isolated active region NOAA AR 7978 in the period of July–November 1996. The number of flares and CMEs which originated from this AR is shown in Table 1. During the emergence and the two following rotations, the AR produced numerous flares (including an X2.6 flare and CME event on 9 July, see Dryer et al. 1998) until the disappearance of the main spots after its third rotation. On the other hand, CME activity, which was at first mainly related to flare events, continued at a surprisingly high level for the next three rotations (van Driel-Gesztelyi et al. 1999), while the magnetic helicity content of the dispersed active region remained reasonably high (Démoulin et al. 2002). However, none of the late CMEs were related to flare events above the GOES B1 level. Table 1 lists the number of flares in different GOES classes and of

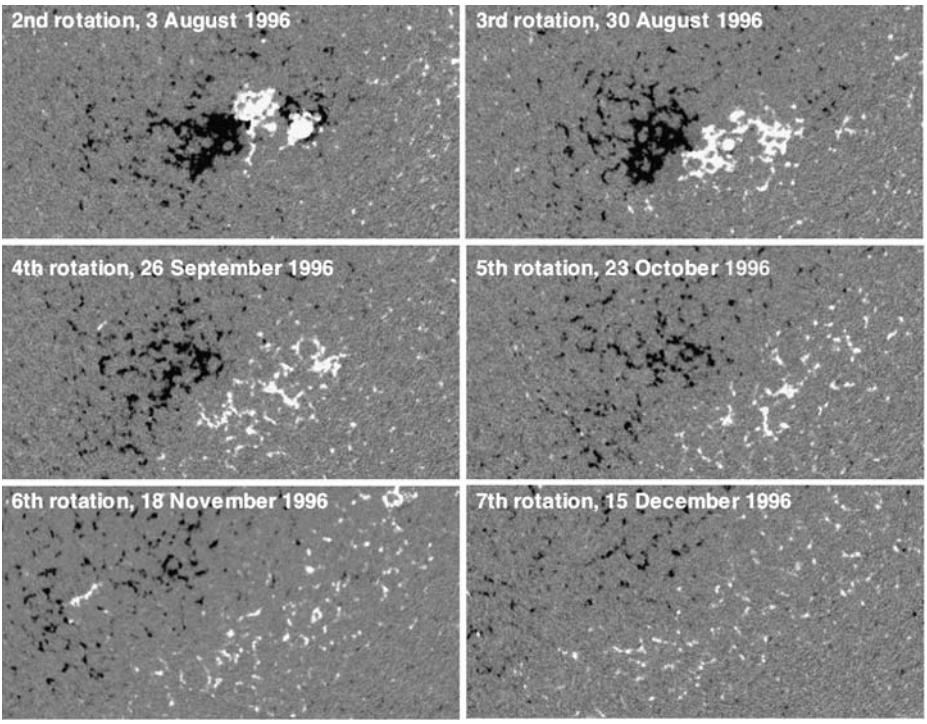

Fig. 1b SOHO/MDI magnetograms showing the decay phase (Rotations 2–7) of NOAA AR 7978 (cf. Fig. 1a) Note the simplification of the magnetic structure with time. Figure adapted from van Driel-Gesztelyi (1998)

the observed CMEs. The flare data in Table 1 was taken from GOES X-ray and optical event catalog (http://www.lmsal.com/SXT/). CMEs have been identified in SoHO/EIT data (Delaboudinière et al. 1995) and SoHO/LASCO (Brueckner et al. 1995) observations by Démoulin et al. (2002). The low level of activity during the lifetime of AR 7978 allowed the identification of even back-side CMEs that originated from this AR when it was on the far side of the Sun. The number of CMEs has been corrected for data gaps assuming that the frequency of the CMEs was the same during the gaps as during observing times (Table 1). This doubles the sampling of CME relative to that of the flares which could only be observed when the AR was on the visible hemisphere.

It is clear from the examples shown in Table 1 that the highest activity occurs during the emergence phase. High magnetic flux density in an AR increases the probability of high reconnection rate in activity events and thus the appearance of bright flare ribbons. CMEs occurring during the decay phase due to filament eruption may well have the same underlying physics, but the accompanying activity manifestation (two-ribbon flare) will be weaker and beyond a certain point into the decay phase even below detection level.

There is a clear consensus linking the energy source of eruptive activity to free energy in the magnetic field. Interesting recent results by Règnier and Priest (2007) compute the altitudes and magnitudes of free energy in an emerging flux region with low magnetic current density and a decaying active region with high current density. The decaying active region has a simple magnetic configuration in which the distribution of strong currents indicate a twisted flux tube with a free energy of 2.6×10^{31} erg (40% of the total energy) stored as

Table 1 Evolution of Flare and Coronal Mass Ejection (CME) activity during the lifetime of an isolated active region NOAA 7978 (July–November 1996; based on Démoulin et al. 2002)

Rotation No.	Day of CMP	Number of flares					Number of CMEs	
		X	M	C	B	Subflare[1]	Observed	Corrected[2]
1st[3]	07 July	01	02	14	11	11	08	11
2nd[4]	02 August	–	–	–	16	01	05	05
3rd	30 August	–	–	01	08	–	02	03
4th[5]	25 September	–	–	–	–	1(?)[6]	05	05
5th	23 October	–	–	–	–	1(?)	03	04
6th	19 November	–	–	–	–	2(?)	03	03

[1]GOES flux is in the B-flare range, but there is no GOES-class given in the list

[2]Corrected for data gaps

[3]Emergence

[4]Peak magnetic flux

[5]Sunspots have disappeared

[6]GOES flux reaches B1 level, but source region is uncertain

high as ∼50 Mm. The weak currents in the newly emerged complex active region do not dramatically modify the connectivity of the magnetic field lines and the magnetic topology of the configuration i.e. the departure from a potential field is small, but the excess magnetic energy of 2.4×10^{31} erg, which represents only 2.5% of the total energy of the AR, is stored in the low corona and is still enough to power flares. Corroborating evidence for low-lying free energy storage in an emerging flux region is provided using non-linear force-free field extrapolations from vector magnetic field measurements. Schrijver et al. (2008) find evidence for filamentary coronal currents located $\leq$20 Mm above the photosphere in an emerging AR 10930 prior to the X-class flare and CME event on 13 December 2006.

4 Relationship of Magnetic Properties to Activity

Less than 10% of the ARs which emerge on the Sun will ever produce a major (M, X) flare (Georgoulis and Rust 2007). However, do we understand what makes one active region produce energetic flares and fast CMEs and another quiet? Which are the distinguishing features of regions of highly activity?

Based on decades-long observations the most frequently mentioned magnetic characteristics of ARs in which large solar flares/CMEs occur are:

- fast evolution (flux emergence)
- large size (high magnetic flux)
- complex magnetic field topology—δ-spots
- long magnetic inversion lines
- high magnetic shear
- strong field gradients
- high helicity and/or high free energy content.

However, which one of these is the most important? Is there one single determining characteristic or is it perhaps a combination of different factors which leads to important

eruptions? Seeking answers to these questions, several groups published series of papers carrying out parametric studies of the photospheric magnetic field in an attempt to find the link with flare and/or CME. Since the proof of the pudding is in the eating, most of the groups expressed the results in probability (success) of forecasting activity events.

4.1 Magnetic Parametric Studies and Short-Term Activity Forecast

K.D. Leka and G. Barnes published a series of papers between 2003 and 2007 in pursuit of finding the best magnetic field parameters for predicting imminent flare activity. In Paper I, Leka and Barnes (2003a) using time-series of photospheric vector magnetic data for three ARs, derived 30 (!) magnetic parameters. The evolution of these was studied in pre-flare vs. flare-quiet periods. No obvious flare-unique signature was found. In Paper II, Leka and Barnes (2003b) took a statistical approach based on discriminant analysis (DA) for 7 ARs in 10 flaring and 14 quiet periods. The conclusions were disappointing: no single parameter appeared to separate reliably the samples of these two populations without producing false alarms. However, when multiple parameters were considered simultaneously, the samples separated in some cases.

In Paper III (Barnes and Leka 2006) coronal topology or complexity was analyzed in a parametric approach using the magnetic charge topology model (Barnes et al. 2005), which separated the two samples more successfully. However, the small sample size prevented them from reaching definite conclusions. In Paper IV, Leka and Barnes (2007) analyzed daily samples of the two populations on a much larger dataset (1200 magnetograms, 496 ARs), and at the small-flare (C1) level the most powerful predictors were found to be two strongly correlated variables: total magnetic flux $\Phi_{\rm tot}$ and total electric current $I_{\rm tot}$. The best discriminant functions resulted from a combination of $\Phi_{\rm tot}$ or $I_{\rm tot}$ with another uncorrelated variable, e.g. magnetic shear (80% success *vs* 70% for flare quiet case). On the larger (M1) flare level excess photospheric energy outperformed other variables (93% success *vs* 90% for flare quiet case). However, they concluded, that "The state of the photospheric magnetic field at any given time has limited bearing on whether that region will be flare productive." Are these negative summed-up results too pessimistic? Perhaps these authors have put the stakes too high, or rather, the flare importance level they wished to predict, too low and were drowned with a large number of photospheric magnetic parameters. Another possible approach is to go only for the big activity events trying to spot some distinguishing differences in the hopefully more important photospheric signatures.

In a series of papers the MSFC group, Falconer, Moore and Gary (Falconer 2001; Falconer et al. 2002, 2003, 2006) explored the significance and correlation of three to six magnetic parameters in an increasingly large sample (4–31) of bipolar ARs and their forecasting power for the occurrence of CMEs. Three of the parameters represented measures of the total non-potentiality of the AR: (i) total length of magnetic inversion lines with high shear (L_{SSM}), and (ii) high gradient (L_{SGM}), and (iii) the net vertical current I_N. Two parameters represented measures of the degree of overall twist: (iv) the 'best' α, $\alpha_{\rm BC}$, and (v) the 'magnetic twist' parameter $\alpha_{IN} = \mu I_N/\Phi$, where Φ is (vi) the total magnetic flux, an independent parameter. They found the best predictive power of parameters for magnetic twist and flux content, but remarked that the total magnetic free energy in an AR is stronger determinant of its CME productivity than is the field's overall twist (helicity) alone. However, recall that a *proxy* was used for magnetic free energy $\alpha_{IN}\Phi$ ($\alpha_{IN} = \mu I_N/\Phi$) and for helicity the "twist" parameter α (while helicity, in fact, rather is $\alpha\Phi^2$). Furthermore, the α parameters used are global ones, disregarding that the twist may be localized in ARs.

Wang et al. (2006) carried out case studies for five ARs which produced six $\geq$ 5X flares. They found that locations of high shear (derived from vector magnetograms) and gradient (from LOS magnetograms) were well correlated ($\sim$90%). Magnetic gradient appeared to be a better proxy than shear for predicting where a major flare might occur. However, it is noteworthy that the mean gradient for these extreme flaring neutral lines was between 0.14–0.50 G km^{-1}, which is 2.3–8 times higher than the usual magnetic gradient values. Horizontal and vertical shearing flows in the vicinity the neutral line prior to and during an X10 flare (Deng et al. 2006) confirm the concentration of free energy on small spatial scales.

The NAO (Beijing) group, Cui et al. (2006, 2007) also analyzed these parameters and their predicting power for flares using 1353 vector magnetograms from Huairou. Using this broader and less extreme sample they found that high-shear and high-gradient neutral lines as defined by the MSFC group for CME prediction appear at about the same time, but they do not overlap much in space. However, the length of their overlap both in space and time gave the best correlation with flare productivity.

The Lockheed group tried to quantify the direct cause of non-potentiality in the active region corona instead of flare forecast. Schrijver et al. (2005) extrapolated the photospheric field to study the deviation of the coronal field in 95 ARs from the potential configuration comparing field lines from potential extrapolations to observed coronal loops (TRACE). They concluded that significant deviation from non-potentiality occurs when (i) new flux has emerged within or very near a region within the last $\sim$30 hr, creating complex polarity separation lines, and (ii) rapidly-evolving opposite-polarity concentrations are in contact at 4″ resolution. As for flare frequency, they found that flares occur 2.4 times more frequently and are 3.3 times brighter (in SXRs) in non-potential ARs, which provides another evidence for the role of free magnetic energy plays in flares.

However, providing flare forecast using a photospheric parameter which can easily be derived from SOHO/MDI LOS magnetograms remained too tempting. Schrijver (2007) took the challenge, and defined a new metric (R) for this purpose quantifying high-gradient strong-field polarity inversion lines. First, in an MDI magnetic map strong positive and negative magnetic areas ($\geq$150 Mx cm^2) are identified using 6″ $\times$ 6″ kernels (2.2×10^{16} cm^2 area). The parameter R is defined as the summed-up flux of the *overlap* between the positive and negative strong-flux areas. Figure 2 shows an example: MDI magnetogram of AR 10720 on 18 January 2005 (left panel; note that in the original paper this AR is mis-identified) and the location of high-gradient, strong-field, polarity-separation lines, which, after summing their absolute values, yields R (right panel). Forecast success of a major flare (M or X GOES class) within 24 hours had a probability of almost 1 when $R \geq 2 \times 10^{21}$ Mx ($\log R \geq 4.8$), while the probability was almost zero when $R \leq 10^{19}$ Mx ($\log R \leq 2.8$). A great advantage of this method is that determination of R is readily automated, making it an effective tool for flare forecasting. The apparent importance of high-gradient strong inversion lines, which are considered as characteristics of emergence of compact electrical currents, provide further evidence for flux emergence in a strongly non-potential state or with twist (helicity) and its importance for eruptive activity.

4.2 Metrics and Effects of Magnetic Complexity

In order to produce a metric for magnetic complexity, Georgoulis and Rust (2007) introduced the effective connected magnetic field of active regions. Building on the magnetic charge topology model developed by Barnes et al. (2005), they resolve an AR having N $(m + l)$ flux concentrations each with a flux Φ_k and centroid position r_k, there are $m \times l$ magnetic connectivities, each having flux of Φ_{ij} with $L_{ij} = |r_i - r_j|$ separation length. The

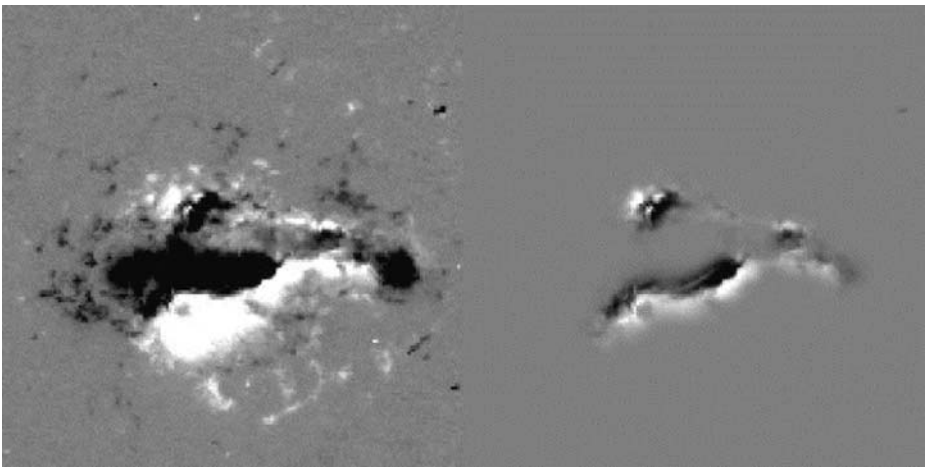

Fig. 2 SOHO/MDI magnetogram of NOAA AR 10720 on 18 January 2005 (*left panel*) and the location of high-gradient, strong-field, polarity-separation lines, which, after summing their absolute values, yields the metric R as proposed by Schrijver (2007) for flare forecast (*right panel*). Figure adopted from Schrijver (2007)

effective connected magnetic flux, $B_{\rm eff} = \sum_{i-l}^{m} \sum_{j-l}^{l} \Phi_{ij} L_{ij}^2$ for $\Phi_{ij} \neq 0$. Calculating $B_{\rm eff}$ for 298 ARs observed between 1996 and 2005, which fell into three groups: 47 and 46 were X-flare and M-flare productive, respectively, and 205 had no major flares, it was found that $B_{\rm eff}$ exceeded 1600 and 2100 G for M and X-class flares respectively, at 95% probability.

Continuing this work, Georgoulis (2008) calculated $B_{\rm eff}$ for 23 CME source regions and studied its correlations with flare magnitude, CME velocity and CME acceleration magnitude, which all seemed to increase with increasing effective connected magnetic field.

4.3 Photospheric Fields Are Relevant, but Are They Sufficient?

Another clue for the role of photospheric magnetic fields in flares is provided by a clear sign that the photospheric magnetic field changes abruptly and non-reversibly during the flare impulsive phase (see e.g. Sudol and Harvey 2005, for a recent survey). Rapid changes in sunspot structure have also been detected by Chen et al. (2007) in 40% of X-class flares, 17% of M flares and 10% C flares.

Free magnetic energy for eruptions is stored in the corona. A typical pre-eruption configuration is a stressed core field (around a high-gradient and high-shear magnetic inversion line) held down by an overlying stabilizing (arcade) field. The latter underlines the importance of a larger-scale magnetic environment in the eruption process.

Whether an eruption fails or succeeds depend on the strength and profile of the overlying fields: rapid decrease, which is typical for complex active regions, being more favorable for full and fast eruption (Török and Kliem 2005, 2007; Liu 2008). Therefore, besides the characteristics of the photospheric magnetic field in an AR one has to assess the coronal conditions as well in order to understand and thus be able to forecast eruptions.

4.4 Helicity Injection, Content and Eruptive Activity

When measurements of the helicity content of active regions became possible, they seemed to bring a crucial factor to understanding the initiation of CMEs.

Andrews (2003) analyzed X and M flares in the period of 1996–1999. The sample consisted of 229 flares with good LASCO coverage. About 40% of M-class flares had no associated CME, while all of the X-class flares were found to be associated with CMEs (however, see Green et al. 2002b for a counter-example). Nindos and Andrews (2004) studied the same data set to find out what the difference is between eruptive and confined big (M) flares, asking the question: is it helicity that makes the difference? They computed coronal helicity content of the ARs using magnetic extrapolations in the linear force-free field approximation fitting computed field lines to observed coronal loops. The two samples appeared well separated: active regions which produced flares with accompanying CMEs had, on average, about a factor of four times more magnetic helicity than the ARs which produced M-class flares without CME, an impressive result.

Barry LaBonte had started a comprehensive project to nail down the role of helicity in eruptive activity events. Unfortunately, his untimely death left the project half-finished (LaBonte et al. 2007; Georgoulis and LaBonte 2007). Using automated processing the photospheric magnetic helicity flux was computed for 48 X-flare producing and 345 non-flaring ARs observed in the period 1996–2005. It was found that most regions grow or decay 10% day^{-1}, except for EFRs, with most of the X-flaring ARs being in growth phase. Causal links were demonstrated between both peak helicity injection rate and 4–7 day helicity changes, X-flaring and CME production. Peak helicity flux prior to X-class flares producing a CME exceeded 6×10^{36} $\mathrm{Mx}^2\,\mathrm{s}^{-1}$.

To the questions 'is large helicity necessary condition for big flare/CME?' or 'What is more important, large free magnetic energy or large magnetic helicity?' We still cannot give a confident answer. A systematic study is still lacking.

5 Eruptions

While there are quasi-steady outflows of matter from the Sun e.g. fast and slow solar wind, and also comparatively low mass transient outflows such as coronal jets, coronal mass ejections (CMEs) represent the principal solar eruptive phenomenon. In these large-scale matter expulsions, around 10^{13} kg of solar material embedded in 10^{20}–10^{22} Mx magnetic flux is involved with a typical total energy of $\approx 10^{25}$ J. The material drives a shock through the corona and into the interplanetary medium (IPM) with velocity of typically 1000 $\mathrm{km\,s}^{-1}$ but ranging up to three times this value. Systematic CME studies began through the use of space-borne coronagraphs with early work being carried out by instruments on the Skylab and Solar Maximum Missions (MacQueen et al. 1974, 1980). Coronagraphs respond to photospheric white light scattered by the expanding ejected material. A typical CME structure is indicated in Fig. 3 while a schematic diagram of the related shock, erupting material, cavity and the underlying prominence is also shown. More recently a substantial body of CME observations, undertaken with the Large Angle Spectrometric Coronagraph on SOHO (Brueckner et al. 1995), has provided considerable new information about these events.

A number of on-disc and low coronal signatures are now recognized as being associated with CMEs. These include prominence or filament eruptions, post-eruption arcades and Moreton waves (Moreton and Ramsey 1960). In addition type II radio bursts (Wild and McCready 1950) have been associated with the propagating CME shock. More recently coronal EUV or X-ray dimmings (Sterling and Hudson 1997) and EIT waves (Thompson et al. 1998) were recognized as being related to CMEs. In addition there have been efforts to characterize particular pre-eruption active region structures e.g. sigmoidal loops (Rust and Kumar 1996; Canfield et al. 1999), as being likely to originate CMEs. An example of CME-related dimmings associated with the flare and CME events of 12 May 1997 (Attrill et al. 2006) is given

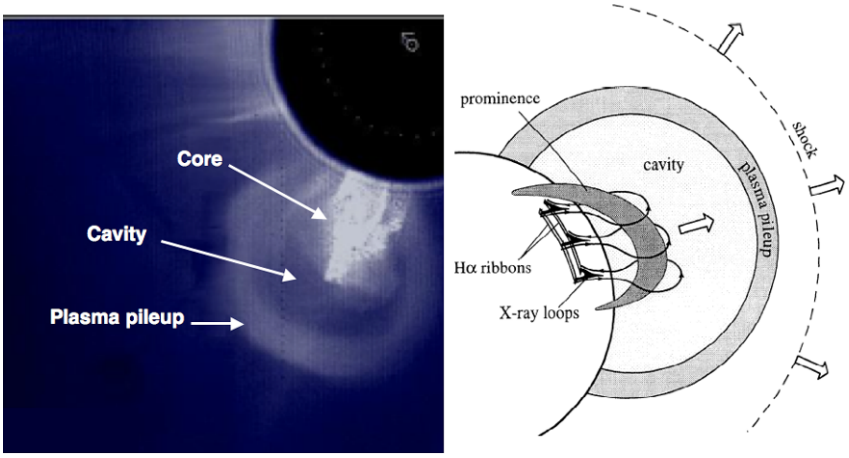

Fig. 3 (*Left panel*) A Solar Maximum Mission archive image showing the principal features of a CME (Hundhausen 1999). (*Right panel*) Schematic view of the CME features (Forbes 2000)

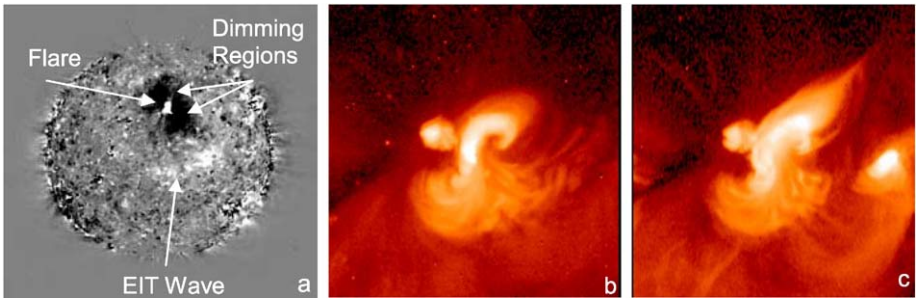

Fig. 4 **a** An EIT difference image showing the flare site, twin dimming regions and the propagating global wave (Attrill et al. 2006). A sigmoid shaped structure associated with the eruptive event of 8/9 June 1998 showing the structure **b** before and **c** after eruption (Glover et al. 2001)

in Fig. 4a. The related global EIT wave is also apparent. A coronal sigmoidal structure eruption is also shown (Figs. 4b, 4c; Glover et al. 2001).

It is generally believed that free energy stored in the magnetic field provides the most likely energy source for these eruptions and that they originate from initially closed non-potential magnetic field that is forced open. Non-potentiality is required as a consequence of the Aly-Sturrock conjecture (Aly 1984, 1991; Sturrock 1991) which asserts that a closed force-free field configuration will always have less energy than the corresponding open field. Magnetic helicity, a quantity that describes the non-potentiality and topological complexity of the magnetic field (Sect. 2.4), is generated in the solar interior and transported to the surface. Magnetic helicity (Berger 1984) is a conserved quantity that emerges with consistent sign; negative in the Northern hemisphere and positive in the Southern, and this pattern does not change with the solar cycle (Pevtsov et al. 2001). Thus helicity accumulates in closed magnetic structures but cannot be eliminated by e.g. flare reconnection, so is probably removed to the IPM by CMEs. The latter also originate in closed structures e.g. active regions, streamers, and are often associated with prominence eruptions.

Eruption models concentrate on explaining how the required energy is stored and how its ultimate release is triggered. Among several reviews of this topic e.g. Forbes (2000), Klimchuk (2001), Zhang and Low (2005), we follow the classification of models suggested by Klimchuk as being i) directly driven or ii) storage and release. Models in category i) include thermal blast where the eruption energy is available from solar flares e.g. Dryer (1982), Wu (1982), and dynamo models e.g. Chen (1989), where rapidly injected magnetic flux further stresses or shears existing field structures. In general, these models cannot easily reproduce the observed features of CMEs or they require unreasonably rapid rates of magnetic flux injection into the corona.

The storage and release models involve energy build up through the stressing of the magnetic field which provides energy to drive the eruption. The involvement of prominences and overlying streamers led to the development of mass loading models e.g. Low and Smith (1993), Low (1996, 1999). Here the already non force-free field of a flux rope is further stressed by the cool prominence mass and the mass of the streamer. Removal of the mass can then lead to the eruption. However not all CMEs have associated prominence mass involved while for those that do, some or all of this mass is often seen to rise as part of the eruption rather than drain away as would be required to unload the stressed configuration. It is also difficult to envisage the conditions of high plasma β and specific coronal mass distribution with high density material overlying low density cavities as are required in the model of Wolfson and Saran (1998). Here again not all CMEs are seen to involve helmet streamers. Thus mass loading models can at best explain only a subset of all CMEs.

Most recently developed models have tended to focus on changes in magnetic structures that are non-potential and therefore have associated free energy that can become available to drive an eruption. Common to all of these models is the progressive build up of free energy and its eventual eruptive release. The structural changes usually involve magnetic reconnection. From the large number of such models that have been developed, we will describe three examples. A model that requires quadrupolar magnetic topology and uses energy stored in sheared arcades—the magnetic breakout model, has been proposed by Antiochos et al. (1999). The progress of energy storage through stressing of a central magnetic arcade and the approach to final eruption are shown in Fig. 5 where four flux systems are involved. Footpoint motions shear the central closed arcade which is inflated by increasing magnetic stress. Reconnection occurs between the expanding arcade field (blue) and the overlying field lines (red). Removal of the overlying field allows further expansion of

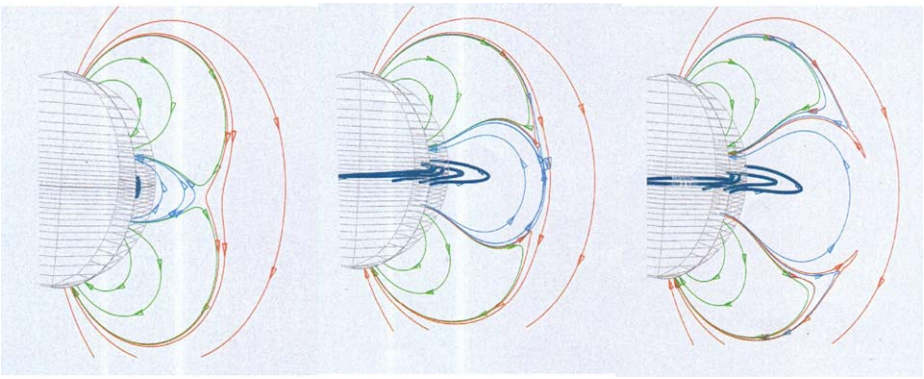

Fig. 5 Stages in the development of a magnetic breakout eruption simulation (Antiochos et al. 1999)

the central sheared arcade which leads rapidly to an eruption driven by the sheared arcade magnetic energy.

Flux cancellation or the mutual disappearance of magnetic fields of opposite polarity at the neutral line separating them (Martin et al. 1985), can lead to sheared field and the creation of a flux rope with associated free energy (van Ballegooijen and Martens 1989). More recent calculations and simulations e.g. Forbes and Isenberg (1991), Forbes et al. (1994), Lin et al. (1998), Linker et al. (2003), have shown that, following the formation of a fluxrope, continued flux cancellations will result in an increasing fluxrope height and a loss of equilibrium. Towards the end of the flux cancellation phase, a vertical current sheet is formed that stretches downwards from the elevated fluxrope. Reconnection at the current sheet allows the eruption to proceed rapidly to completion. This reconnection leads to the formation of a closed loop arcade underneath the erupting fluxrope that grows with time.

The third kind of model for eruptions involves the operation of ideal MHD instabilities e.g. the kink and torus instabilities. The kink instability occurs in a flux rope when the twist exceeds a critical value leading to a helical deformation of the flux rope's axis (Hood and Priest 1981). Using the loop model of Titov and Démoulin (1999) as a starting point, Török et al. (2004) and Török and Kliem (2005) have simulated the kink instability. They use their simulations to reproduce both confined (27 May 2002) and completed (15 May 2001) eruptions and show that a steeper decrease of magnetic field with height in the corona above the flux rope can allow the full eruption to proceed. Fan (2005) has also simulated the kink instability and showed that transient S- or sigmoid-shaped structures can develop during eruption onset similar to those observed in some flares and CMEs e.g. Sterling and Hudson (1997). Williams et al. (2005) have compared an observation of a filament eruption observed by TRACE on 2004 November 10 with the simulation of Török and Kliem (2005). Stages of the eruption are compared with the simulation in Fig. 6 where the qualitative agreement is apparent. However for this event, which takes place in a quadrupolar magnetic configuration, it is likely that elements of both the flux cancellation and breakout models may also have been involved in weakening the restraining fields before the kink instability finally became the principal driver of the event.

A current carrying ring situated in an external poloidal magnetic field ($B_{\rm ex}$) is unstable against radial expansion when the Lorentz self-force (hoop force) decreases more slowly than the stabilizing Lorentz force due to $B_{\rm ex}$. Known as the torus instability, its possible role in solar eruptions has been examined by Kliem and Török (2006) while an MHD simulation based on a line tied flux rope (Titov and Démoulin 1999) was done by Török and Kliem (2007). With $B_{\rm ex} \approx R^{-n}$, they establish that $n > 3/2$ is the threshold for instability onset and that with an appropriate starting height for the curved flux rope, the eruption acceleration depends on the steepness of the radial field gradient. Thus CMEs from complex active regions with steep field gradients in the corona are more likely to give rise to fast CMEs—something that is indeed observed.

While there is often a compulsion to establish a single energy storage and release model as being the cause of eruptions or CMEs, given the complexity of the magnetic topologies it would not be surprising if elements of several models were involved. Thus we have seen that separate means for weakening the fields that restrain fluxropes may still play a role in situations where the kink instability emerges as the principal driver of the eruption. For the MHD instabilities, the kink process which is commonly thought more likely to cause confined eruptions, may establish the initial conditions where a complete eruption can continue through the operation of the torus instability. Line tied fluxropes clearly play an important role both for containment of cool prominence material and as erupting flux configurations even in cases where no prominence material is present. For both the magnetic breakout and

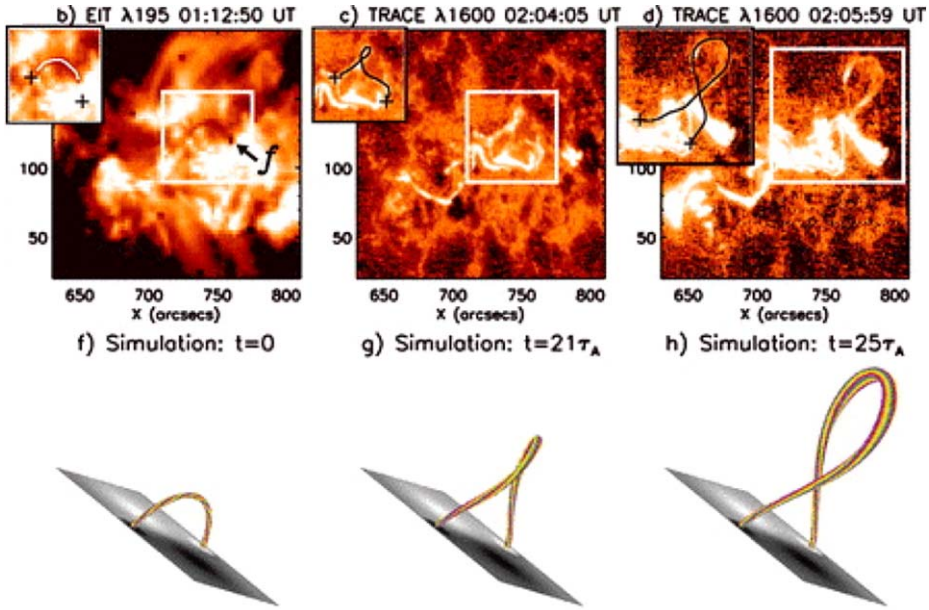

Fig. 6 Panel **b** shows a pre-eruption EIT image while panels **c** and **d** are TRACE images that show the eruption of a heated kinked filament (Williams et al. 2005). Panels **f**, **g** and **h** illustrate the progress of the kink instability from a numerical simulation by Török and Kliem (2005)

flux cancellation models, fluxropes are formed during the energy build up phase or in the course of the eruption. The MHD instabilities could be initiated by adding twist or curvature to a pre-existing fluxrope or to one that had previously emerged. However it is difficult at present to observationally establish the origins of fluxropes later seen in the IPM.

6 Interplanetary Coronal Mass Ejections and Magnetic Cloud Characteristics

Following an eruption or CME on the Sun, plasma and magnetic field expand into interplanetary space behind a propagating shock. The resulting structures are called Interplanetary CMEs (ICMEs). The term Magnetic Cloud (MC), where a more restricted set of characteristics is present, is used for a subset of these cases. Thus for in-situ observations at ≈ 1 AU distance from the Sun, the cloud will exhibit a stronger magnetic field than the surroundings (Hirshberg and Colburn 1969), lower temperature and plasma β values (Gosling et al. 1973) and a smooth rotation of the magnetic field (Klein and Burlaga 1982).

It is important to relate the properties of the MC to those of the original eruption. Relevant parameters for comparison include i) magnetic field direction, ii) magnetic flux, iii) magnetic helicity and iv) plasma composition. At present coronal *magnetic field direction* is usually inferred from extrapolations of photospheric field measurements but in an eruption, field strength and direction can change rapidly (see Fig. 6). A CME is typically not identified in a coronagraph image until ≈ 20 min after its launch. Related surface phenomena e.g. coronal dimming outflows, can however be identified and associated with the footpoints of the erupting structure. This can in turn allow the *magnetic flux* associated with the dimming regions to be estimated but we will see below that the relationship with magnetic cloud flux is not

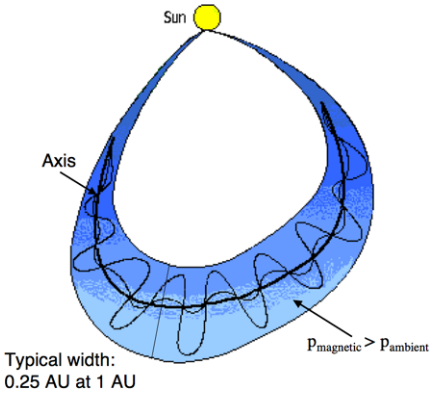

Fig. 7 Schematic diagram of a magnetic cloud showing the geometry and a typical scale. The helical magnetic field lines of the flux rope configuration are indicated. Both ends of the flux rope are connected to the Sun (adapted from Webb et al. 2000)

always simple. *Magnetic helicity* as a conserved quantity preserves its sign and magnitude. Sign can be inferred from vector field measurements at the eruption site or from the orientation of observable structures in the chromosphere and corona. Following the definition of relative helicity (Berger 1984) the change in helicity in the corona following an eruption can be calculated and compared with the value in a MC. It is difficult to determine *plasma composition* in the erupting material for later comparison with that detected at around 1 AU since there are many possibilities for changes to occur in transit. Thus such comparisons tend at present to be made in a qualitative manner.

A schematic diagram of a MC is shown in Fig. 7. The observed rotation suggests that the cloud field configuration is that of a fluxrope which has expanded with the original CME (see Figs. 1a and 1b). In-situ measurement of the field is typically made by magnetometers on a single spacecraft which, for best advantage would pass close to the cloud axis. In such an encounter the direction of the fluxrope axis can be established by a minimum variance analysis. Somewhat better estimates may be obtained by fitting different fluxrope models to the magnetometer data and comparing the results (Dasso et al. 2005). For encounters with high impact parameter, it is necessary to proceed by applying different models. A typical sample of in-situ data from the WIND spacecraft is shown in Fig. 8. The upper panel indicates the sudden increase in plasma velocity that accompanies the arrival of the shock. This is followed by an interval of swept-up solar wind or sheath plasma. Within the cloud, a significantly reduced density is observed in the second panel of the figure while the next three panels show the characteristic magnetic field rotation that characterizes the fluxrope structure. Comparison of cloud axis directions, measured in-situ, with that of the original erupting filament channel or prominence reveals a wide range of behavior. In many cases there is good agreement between these directions (Marubashi 1997; Bothmer and Schwenn 1998) but in others, rotations range from a few tens of degrees (Marubashi 1997; Zhao and Hoeksema 1998) to 130–160 degrees (Rust et al. 2005; Harra et al. 2007). Development of a full kink instability, where magnetic helicity is transformed from twist to writhe may be responsible for the extreme values. The event shown in Fig. 6 provides a possible example of this behavior.

The schematic of Fig. 7 shows both ends of the cloud connected to the Sun. In-situ observation of counter-streaming supra-thermal electrons in a cloud is usually taken to indicate that the cloud or fluxrope is connected at both ends (Richardson et al. 1991; Richardson 1997). The bottom panel of Fig. 8 shows an in-situ electron analyzer spectrogram where the electrons are widely distributed in pitch angle indicating the presence of bi-directional electron streams. Conversely the absence of such electron streams suggests

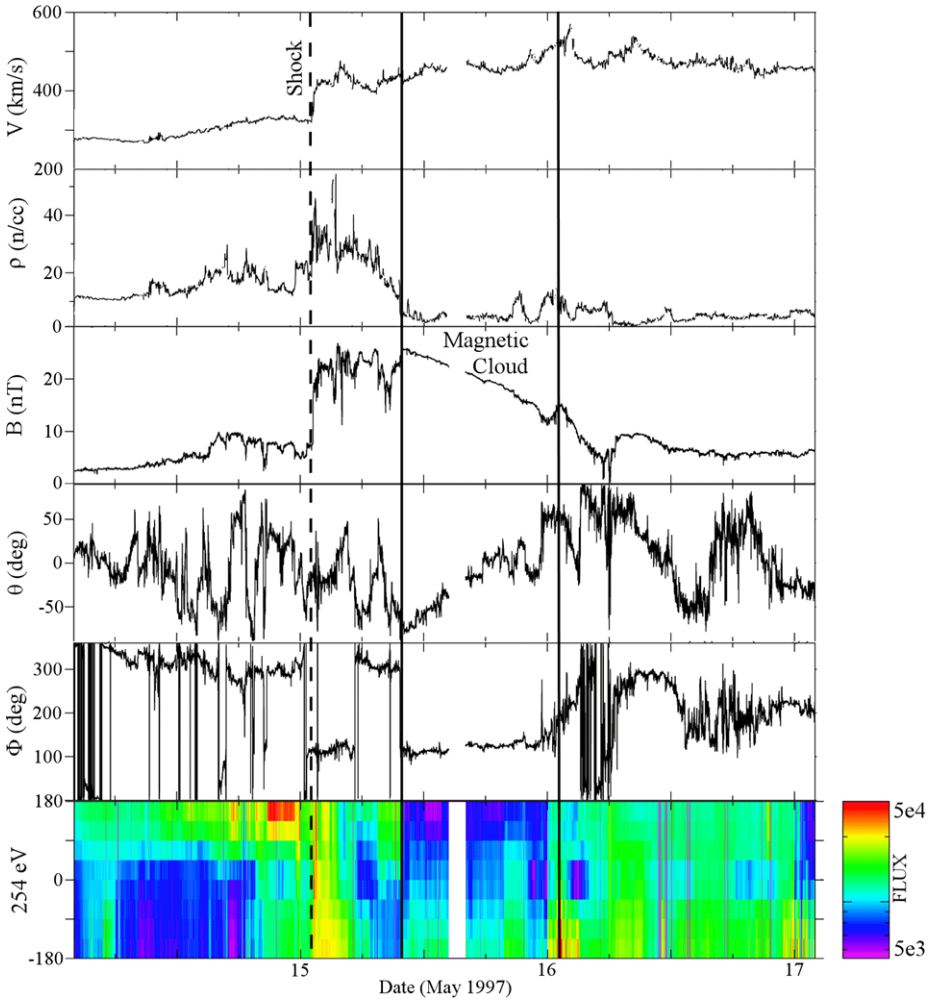

Fig. 8 In-situ observations of a magnetic cloud from the WIND spacecraft. *Panels from the top* give solar wind velocity (V), plasma density (ρ), magnetic field strength (B), elevation (θ) and azimuth (ϕ) of the field direction in solar ecliptic coordinates. The *bottom panel* shows the electron intensity distribution in pitch angle. The broad distribution indicates the presence of bi-directional electron flows. The arrival of the shock and the passage of the cloud are shown by *vertical lines* on the plots

complete disconnection while a uni-directional electron flow points to the cloud being connected to the Sun at one end only. While the flux rope may be initially connected at both ends, its topology may be modified due to reconnection in the corona with e.g. streamer structures, or by reconnection with interplanetary solar wind magnetic field. The connection topology will clearly impact the associated magnetic flux.

Since the usual interpretation of the coronal dimming regions is as sites of material outflow (Hudson et al. 1996; Harra and Sterling 2001) and two prominent regions are often located on both sides of the eruption site, it has frequently been assumed e.g. Webb et al. (2000), that the dimming regions are at the ejected flux rope footpoints. Magnetic flux at the dimming regions may be measured from magnetogram images and compared with the flux

associated with the related cloud. Axial and azimuthal magnetic flux determination usually requires deduction from in-situ magnetometer data by fitting a magnetic model of the cloud (Dasso et al. 2005) where knowledge of MC axis direction and an assumption of the cloud length are also required. Comparisons often show rough agreement between dimming region and cloud axial fluxes where the latter are estimated from near-Earth in-situ data e.g. Lepping et al. (1997), Webb et al. (2000). However structures observed in interplanetary space are often highly twisted and many clouds have substantial azimuthal flux. Twist may be added following reconnection in a sheared arcade overlying an expanding flux rope (Mandrini et al. 2005; Attrill et al. 2006) in a manner that allows the open flux from the dimming regions to contribute to the cloud azimuthal flux component. It is nevertheless not always possible to relate the dimming region flux to that observed in the MC. Mandrini et al. (2007) have studied an eruption where they find no agreement between the MC flux and that of the multiple dimming regions involved. Thus when comparing solar fluxes with those observed in MCs, the magnetic context of dimming regions and their relation to the eruption involved must be considered carefully.

As described in Sect. 2.4, magnetic helicity, H, quantifies how the magnetic field is sheared and twisted compared to its lowest energy state of a potential or current-free field. The value of the helicity content of active regions as a pointer to their activity is discussed in Sect. 4.4. As a conserved quantity it has an important role in comparisons between eruptions and their related MCs. Thus it is increasingly believed that source region helicity is removed from the Sun in CMEs and is found as a measurable quantity in MCs. Using the methods outlined in Sect. 2.4, the helicity content of an AR can be calculated based on magnetic field extrapolation and the change in helicity from before to after the eruption of a CME can be estimated. As was the case for magnetic flux, the helicity of a magnetic cloud can also be estimated by fitting a model to the MC in-situ magnetometer data or in cases of low spacecraft to cloud impact parameter, H may be derived directly from the data (Dasso et al. 2006). Comparison of the helicity change in the source region with the value measured for the cloud provides insight into the eruption physics and offers a useful aid in matching eruption and cloud identities. These methods are increasingly being used in CME/MC studies and we will discuss an example in Sect. 7.

Although an apparently simple picture of the eruption near the Sun is usually presented (see Fig. 3), the determination of the composition and temperature distribution of the plasma involved is by no means straightforward. Assuming that the eruption involves a flux rope topology, with or without contained filament material, the expanding shock can sweep up a range of possible plasmas in the overlying corona. These may include material from active region loops ($T \sim$ 2–5 MK), flare heated plasma ($T \sim$ 20–30 MK), along with streamers and other quiet Sun structures ($T \sim 1$ MK). In cases where filament or prominence material is involved, the temperature would typically be ~ 0.1 MK. However dark filaments, seen in Hα can also "disappear" before eruption with the plasma becoming visible in emission lines with maximum abundance temperature ranging from He II (0.18 MK) to Fe X (1.0 MK) and above (Tripathi et al. 2008). The situation is further complicated by the partial filament eruptions that are frequently observed. CME magnetic structures may also reconnect with structures in the upper solar atmosphere or in the solar wind that have oppositely directed magnetic fields. This will lead to mixing of the original source region plasma with material that did not participate in the eruption. When this happens below the threshold height of a few $R_\odot$ at which temperature "freeze-in" occurs (Hundhausen et al. 1968), the plasma ion composition will be altered. The plasma may undergo further selective modification by diffusion across field lines during its passage from the Sun which leads to e.g. an enhanced heavy ion concentration (Wurz et al. 2000).

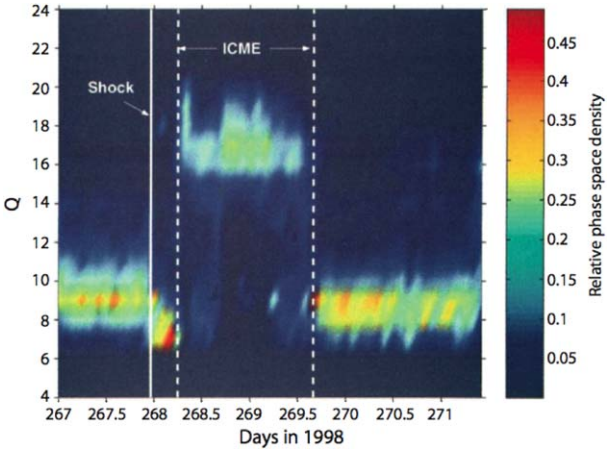

Fig. 9 A broad range of Fe charge states observed from ACE in the period 24–28 September 1998 by Lepri et al. (2001). The shock arrival and ICME passage are indicated by *vertical lines*

Although MCs are identified in only 50% of ICMEs, their magnetic characteristics make it easier to relate in-situ observations to remote observations of the original eruptions. However both ICMEs and MCs exhibit similar composition characteristics. Ion composition and inferred element abundance measurements are made by ion mass spectrometers e.g. the SWICS instruments on the Ulysses and ACE spacecraft and CELIAS on SOHO. In-situ signatures that are of relevance for eruptions at the Sun have been summarized in a review by Zurbuchen and Richardson (2006) for ICMEs and include a) elevated oxygen charge states, $O^{7+}/O^{6+} > 1$; b) average Fe charge state $(Q^{Fe}) > 12$ or $Fe^{\cdot 16+}/Fe_{Total} > 0.1$; c) detection of He^+; $He^+/He^{2+} > 0.01$ and d) high $^3He/^4He$; $(^3He/^4He)_{ICME}/(^3He/^4He)_{photosphere} > 2$. Such signatures are taken to indicate the passage of an ICME or MC and they can at least be qualitatively related to the plasma in the original eruption. Thus Richardson and Cane (2004) in an extensive study have found a) to be a reliable ICME indicator. The elevated Oxygen charge states indicate plasma with $T > 2$ MK and since this value is frozen in below 1 $R_\odot$, it probably reflects an origin in coronal active region structures overlying the eruption site that have been swept up in the expansion of the CME shock.

For indicator b), Richardson and Cane have also demonstrated an association with ICMEs in approaching 70% of the cases they studied. Lepri et al. (2001), have observed a range of Fe charge states from Fe^{+15} up to Fe^{+19} for an ICME seen at ACE during September, 1998 (Fig. 9). This observation shows clearly how the ionizations stage varies from the front (highest) to the back (lowest) of the MC and indicates freeze-in temperatures in the range 2–8 MK. Given that for Fe ions, freeze-in typically occurs at heights up to 4 $R_\odot$, it is clear that the higher temperature material in particular probably originated as 10–20 MK heated plasma from a solar flare associated with the original CME. Assuming a magnetic connection to the CME flux rope or that hot plasma was swept up by the expanding shock, the high Fe stages clearly show a flare-CME association in these cases (Lepri and Zurbuchen 2004).

Indicator c) denotes an enhanced presence of singly charged He. This is seen in a comparatively small number of MCs and suggests the presence of filament material with $T \sim 0.1$ MK (Gosling et al. 1980; Gloeckler et al. 1999). Enhancement of indicator d), suggestive of chromospheric material which would likewise form part of a filament, is observed along with enhancement of He^+. Burlaga et al. (1998) observed a MC for which the rear part of the cloud showed a high density along with enhancements of He^{++}, He^+ and the presence of O^{5+} and Fe^{5+}. This composition suggests freeze-in temperatures of ∼0.1–0.4 MK

characteristic of a filament that may have experienced some heating just before or during the eruption. Given the broad range of plasma compositions and temperatures likely to be involved in the original eruption, the in-situ determination of MC composition and ion stage distribution can provide valuable information on the CME process at the Sun and help to constrain the range of eruption models.

7 Coronal Mass Ejections: From Sun to Earth

As discussed in the two sections above, comparison of the original eruption at the Sun with the behavior and properties of the ejecta in interplanetary space can usefully clarify understanding for both phases. Since a significant minority of CMEs reach the Earth and interact with its magnetic and plasma environments, such studies—often described under the general heading of "space weather", are also valuable in clarifying the CME-Earth interaction and the impact on the near-Earth environment.

In seeking to associate the arrival of a shock front and its associated magnetic cloud at Earth with an eruption that would have occurred $\sim$ two days previously at the Sun, the shock propagation speed is clearly an important parameter. The dynamic spectra of slow-drift type II radio bursts, generally attributed to shock-accelerated electrons (Wild and Smerd 1972), can provide estimates of shock velocity. Since the radio emission is due to local plasma oscillations excited by the passage of the shock where the oscillation frequency is $f_p = 9000\sqrt{n_e}$, the drift rate of the burst to lower frequency can give the shock velocity provided that the electron density of the medium through which the shock propagates is known as a function of distance from the Sun. Frequently used n_e–h models for the corona are those of Newkirk (1961) and Saito (1970) but they predict high n_e values at 1 AU. Since it is important to track interplanetary type II bursts to the neighbourhood of Earth, hybrid density models e.g. Vršnak et al. (2004), are used for connecting bursts in the corona and in interplanetary space. Observations of bursts are made at decimeter–meter wavelengths in the solar atmosphere using ground-based radio telescopes and at decametric–hectometric wavelengths in the interplanetary medium where space-based antennae are required. Uncertainties in the n_e values make it important to assess carefully any speed estimates based on type II burst observations.

Coronagraphs allow measurement of CME speeds in the plane of the sky but in cases where the CME is directed towards Earth—the so-called halo events, determination of the radial velocity is required for estimates of the transit time. It has been pointed out by Dal Lago et al. (2004), that the expansion speed, $V_{\rm exp}$ or the CME lateral growth speed may be determined uniquely for all types of CME. Based on these ideas, Schwenn et al. (2005) have established an empirical relation between the radial and expansion velocities or $V_{\rm rad} = 0.88 V_{\rm exp}$ with a correlation coefficient of 0.86. However the resulting radial velocities apply comparatively close to the Sun. For slightly asymmetric halo CMEs where the launch site is not at sun center, the cone model of Michałek et al. (2003) may be used to estimate radial velocity. The model assumes constant velocity and relies on the time difference between first and last appearance of the CME edges in the coronagraph. The need for asymmetry limits the number of events for which the cone model may be used while the comparatively poor time cadence of current coronagraphs e.g. SOHO LASCO, limits its accuracy.

At distances of $\sim$20–220 $R_\odot$ from the Sun, interplanetary radio scintillation (IPS) observations which exploit the scattering of radiation from distant radio sources e.g. Quasars, by density irregularities in the solar wind, can be used to assess the density-turbulence condition of the ambient solar wind (Tappin 1986; Manoharan 1993). For moving ICMEs, IPS

measurements can easily detect the excess turbulence produced in the ICME sheath or region of compressed solar wind plasma between the shock and the driving cloud (Manoharan et al. 1995, 2000). When coupled with LASCO observations, the IPS measurements are extremely valuable in establishing speed–distance profiles out to beyond 1 AU. They observe in particular the deceleration of faster CMEs by interaction with the ambient solar wind plasma. However comparatively infrequent sampling—three to four velocity measurements during a CME Sun–Earth transit are typical, limits the applicability of the method.

The in-situ observations by near-Earth spacecraft e.g. ACE, Cluster, can register the arrival of CME-related shocks and their associated material. Arriving shocks are detected as sharp increases in solar wind speed as measured by ion spectrometers (see Fig. 8, top panel). Immediately behind the shock, turbulent sheath or swept-up solar wind material is detected. Finally some five to ten or more hours later, the driving coronal ejecta arrive. The time of shock arrival may be related to the CME launch time in order to deduce an average transit speed assuming that a correct association can be made between shock and CME.

As will be clear from the above comments, the estimation of CME transit speed in the interplanetary medium is not a straightforward matter. Thus a combination of the above approaches will usually be required to achieve a reliable outcome. While obtaining a reliable estimate of CME transit time from Sun to Earth is a necessary part of relating observations of the original eruption to the in-situ identification of the associated magnetic cloud or ICME near-Earth, progress in understanding requires a detailed comparison of the parameters of the eruption e.g. magnetic flux, helicity, as described in Sect. 5 with those later measured for the magnetic cloud in the neighbourhood of Earth. We will now seek to clarify this relationship with reference to some sample events.

Mandrini et al. 2005, have observed an unusual eruption at $\sim 09:00$ UT on 11 May 1998 associated with a small bipolar X-ray bright point. An overview of the launch of the fluxrope and the detection of a small magnetic cloud at Earth over four days later is given in Fig. 10. The MDI magnetogram (Fig. 10a) shows the small bipole located near disc center. Its evolution was followed from 9 May and an apparent rotation of magnetic polarities was probably due to the emergence of a strongly twisted flux tube. This is supported by the observation of a sigmoidal appearance in the coronal structure above the bipole as seen in EIT 284 Å images. The modelled magnetic field in the corona also showed an unusually high degree of non-potentiality. X-ray emission from this small region was observed with Yohkoh SXT (Fig. 10b). Three impulsive events were seen and the third of these, which lasted for three hours, had the largest time-integrated X-ray flux. During this latter event, significant changes occurred in the small coronal structures seen with EIT and a cusp formation was also observed. Dimming regions associated with the third event are shown as contours overlaid on an MDI magnetogram in Fig. 10c. In addition to two concentrated regions close to the bipole, there are extended regions that cover a larger area of quiet Sun. From careful measurement of the net magnetic flux associated with the dimming regions, Mandrini et al. obtained a value of $13 \pm 2 \times 10^{19}$ Mx of which about 8% was contributed by the extended quiet region dimming. They also calculated the change in coronal relative magnetic helicity before and after the event. This was based on a linear force free field model where $\nabla \times B = \alpha B$ and best-fitting α values were found by comparing the extrapolated field with the coronal loop structures as seen in the TRACE images. The resulting helicity change was in the range $-3.3 \times 10^{39}\ \mathrm{Mx}^2 \leq \Delta H_{\mathrm{corona}} \leq -2.3 \times 10^{39}\ \mathrm{Mx}^2$.

In order to search for a matching in-situ signature, WIND data were examined by Mandrini et al. for an interval two to five days after the small event on 11 May. A small magnetic cloud—probably the smallest ever observed, was registered by the spacecraft in the interval 22:00 UT to 01:50 UT on 16 May. The characteristic smooth rotation of the magnetic field,

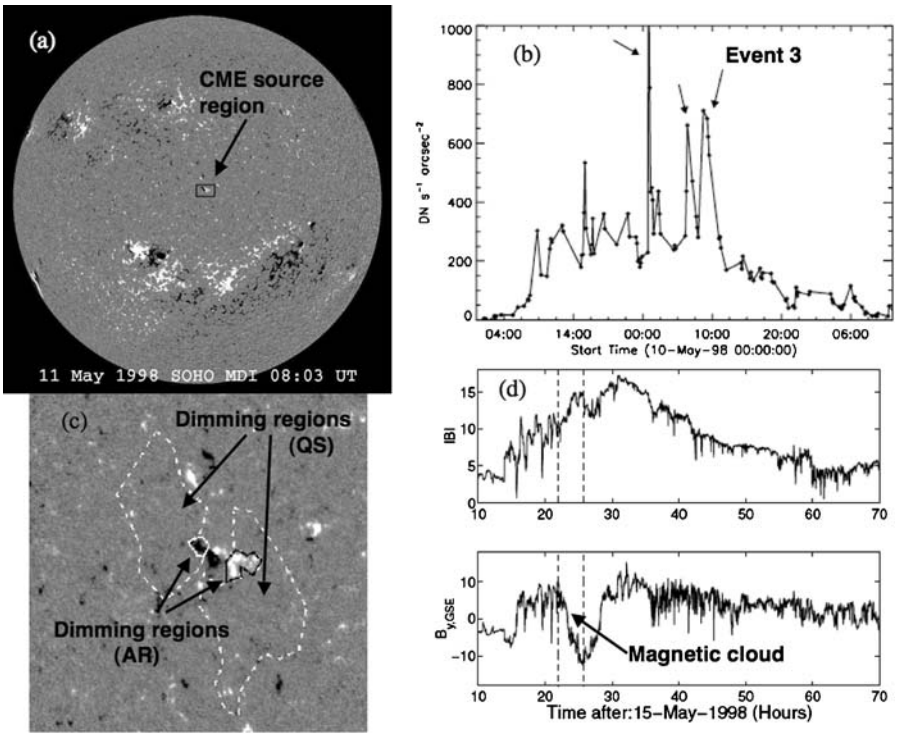

Fig. 10 Observation of a small eruption on 11 May 1998 by Mandrini et al. (2005). The MDI magnetogram (**a**) shows a small bipole near disc center. A Yohkoh SXT X-ray *light curve* (**b**) indicates three small events the last of which relates to the eruption. Associated dimming regions deduced from EIT 195 Å observations are shown in (**c**) while WIND observations on 15 May 1998 of magnetic field for the associated magnetic cloud are in (**d**)

B_{yGSE} shown in the lower panel of Fig. 10d, is consistent with a cylindrical fluxrope crossing the spacecraft. High magnetic intensity and low proton temperature, good indicators of a cloud (Burlaga et al. 1981) were also present. Though no associated CME was observed at the Sun on 11 May, it was presumed that the cloud progressed at the current solar wind speed of 350 ± 50 km s^{-1}. The resulting transit time is 119 ± 17 h while the elapsed time from the relevant solar event to cloud arrival was 110 h. Using the methods described by Dasso et al. (2003), the cloud magnetic field axis direction was determined along with the cloud field and the sign of the twist and helicity. All were consistent with those of the pre-eruption coronal sigmoid structure. Finally the value of magnetic flux ($10–20 \times 10^{19}$ Mx) associated with the cloud was consistent with the net flux associated with the coronal dimming regions while the cloud helicity value (-1.5×10^{39} Mx^2 to -3.0×10^{39} Mx^2) agreed with the pre- to post-eruption helicity change in the corona deduced from the magnetic field extrapolations at the Sun. Thus an unusually good agreement was established between the magnetic properties at the eruption site and those of the corresponding magnetic cloud that was observed near-Earth.

Although the above small event conforms well to the idea that erupting fluxrope footpoints are associated with dimming regions symmetrically located on opposite sides of an active region, this is by no means always the case. The well studied C 1.3 flare event of 12 May 1997 (Webb et al. 2000), with a full-halo CME and an associated magnetic cloud at

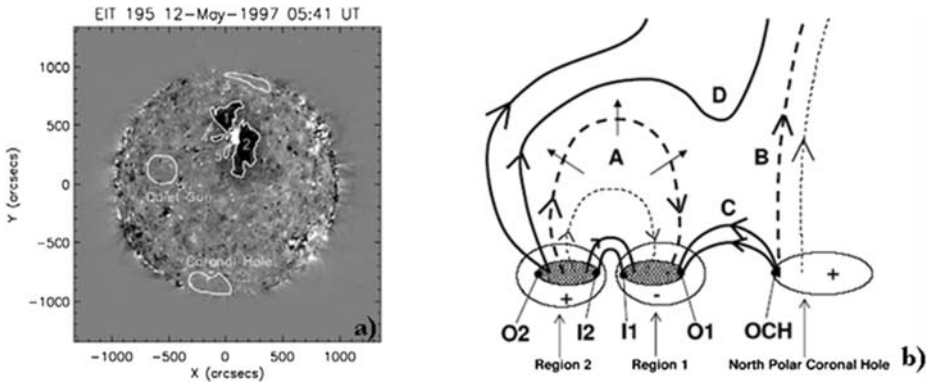

Fig. 11 **a**) EIT 195 Å base difference image at maximum dimming extent. The principal regions are labeled *1* (north) and *2* (south). The North-polar coronal hole is also indicated (Attrill et al. 2006). **b**) Sketch of the evolution of the global magnetic topology for the 12 May 1997 CME and its reconnection with open field lines of the North-polar coronal hole. *Dashed lines* show pre-reconnection magnetic structures, *solid lines* show the post-reconnection fields and *hashed areas* show the main dimming regions. Other symbols are discussed in the text

Earth, was at first thought to conform fully to the twin dimming region scenario. While the magnetic flux associated with the dimming regions was twice that for the related magnetic cloud, only the axial flux component was considered. However the bi-directional electron streaming signature, usually found when both fluxrope legs are connected to the Sun, was not observed.

More recently Attrill et al. (2006), have re-examined this event. The principal dimming regions, labeled 1 and 2 are shown in the EIT 195 Å image of Fig. 11a. From a careful analysis of the time evolution of the two principal dimming regions, Attrill et al have reconstructed the global magnetic topology of the event. A schematic diagram is given in Fig. 11b. While the initial eruption did indeed involve fluxrope connection to regions 1 and 2, the expanding field labeled A reconnected with the open field B of the north polar coronal hole (OCH) to form the magnetic field systems C (closed) by connection to the outer boundary of region 1 (O1) and D (open) which originates from the southern boundary of region 2 (O2). The hot loops that comprise system C are in fact visible in an SXT X-ray image. Progressive reconnection from O1 closes down region 1 which is observed as a shrinking of the region in a plot of dimming recovery. However because of the newly forming open field system D, the southern region 2 remains open for longer. The post-eruption flare loops form between I1 and I2. From the MDI magnetograms, the net magnetic flux from region 2 is $(21 \pm 7) \times 10^{20}$ Mx.

In-situ observations of the related magnetic cloud near-Earth were again obtained by the WIND spacecraft. The observation of uni-directional electron flows suggests that at the time of these observations, the cloud was connected only to the southern region 2. Taking account of the probable time of disconnection from region 1 and of additional path length introduced in the newly opened field from region 2, the cloud length was estimated as 1.3 AU. Fitting magnetic models to the in-situ data as the WIND spacecraft encounters the cloud yields the cloud axis direction which is consistent with the above magnetic topology at the Sun. The total magnetic flux (axial and azimuthal) associated with the cloud is estimated from the best fitting model as $(22 \pm 9) \times 10^{20}$ Mx for the assumed length of 1.3 AU. This figure is in excellent agreement with the southern dimming region flux.

Although the magnetic topology of the 12 May 1997 eruption differs from that of the small eruption of 11 May 1998 that was discussed previously, it was nevertheless possible to relate the magnetic flux associated with a single dimming region with that of the related magnetic cloud. However for the X17 flare and eruption of 28 October 2003, studied by Mandrini et al. (2007), it was not possible to establish any correspondence between the magnetic flux observed in multiple dimming and in the related magnetic cloud. Here the main dimming regions were probably masked by the high flare brightness. In addition the strong lateral expansion of the erupting field reorganized magnetic connectivities which caused the spread of dimming regions over a large part of the Sun (Attrill et al. 2007). Thus the magnetic topology and evolution of each eruption must be studied carefully before any attempt is made to relate the dimming flux and other magnetic properties of the eruption with those of the resulting magnetic cloud. It is clear that such comparisons will be more easily achieved for smaller events than for the eruptions associated with very large flares.

8 Conclusions

The most important characteristic of emerging flux relevant for eruptive activity is that it appears from the solar interior in a non-potential state. Emergence of major concentrated current-carrying (twisted) flux and high photospheric helicity flux show the strongest correlation with major flares and fast CMEs and has therefore the best predictive power. Concentrated current-carrying (high-helicity) flux is characteristic of a flux rope, so big flare and fast CME forecasts provide circumstantial evidence that flux rope emergence plays important role in these activity events. Helicity injection curves in emerging flux regions (e.g. Chae et al. 2004) show a conspicuous peak during the first few days, which greatly resemble the behavior of helicity flux in 3-D MHD simulations of emergence of a twisted flux tube (Cheung et al. 2005). Emergence of a flux rope has many caveats, e.g. dense plasma accumulation in its field lines located under the axis of the flux rope, and a steep gradient in physical parameters leading to strong fragmentation just under the photosphere. A successful emergence must involve many episodes of magnetic reconnection (Pariat et al. 2004). However, characteristic polarity distribution patterns of longitudinal magnetic field in emerging flux regions, the so-called magnetic tongues, indicate that there is an overall organization of the emerging flux tube, which is compatible with a (modest) global twist (Démoulin and Pariat 2008). There are some doubts as to whether or not a flux rope can possibly emerge as an entity. However a weak flux rope emergence may have been seen in Hinode SOT (Tsuneta et al. 2008) vector magnetic data (Okamoto et al. 2008).

During the decay phase of ARs CME activity is maintained (slow CMEs accompanied by small flares, e.g. Démoulin et al. 2002). The AR assumes a simple magnetic configuration, but relatively high current densities indicate an overall flux-rope structure with free magnetic energy stored higher than in an emerging active region (Règnier and Priest 2007). Forecasting methods developed for young ARs would not work for these slow CMEs, however.

It is remarkable that flux ropes are involved in all currently favoured models of CME. The models differ on the nature of the trigger only. Flux emergence and/or flows are implicated in the increase of shear, twist, and complexity, while tether cutting and breakout in changing the overlying field strength. Kink instability can lift the flux rope, facilitating torus instability. There is no consensus among the modellers over the origin of flux rope, whether it pre-exists or forms during the eruption. It seems, however, that during the eruption magnetic reconnections increase its twist (Démoulin 2008; Gibson and Fan 2008). Photospheric

magnetic field typical of pre-eruption conditions seem to favour the pre-existence of a flux rope in the AR.

The CME eruption—and any associated solar flares, represent the last stage in the progression of magnetic flux from the Sun's interior to its outer atmosphere. The need to occult the solar disk poses a problem in searching for associated photospheric, chromospheric and lower coronal phenomena. Nevertheless considerable progress has been made in this area, principally through observations by the Yohkoh, SOHO, TRACE and more recently Hinode and STEREO missions. Use of the SOHO EIT and LASCO instruments has been most relevant but their comparatively low time cadence has led to difficulty. While models involving the storage of free magnetic energy and its later release through a triggered instability are becoming generally accepted as providing the basis for understanding eruptions, the observational difficulties mentioned above make it difficult to establish valid and complete explanations. The situation is further complicated by evidence that different models may be appropriate for different events and, in some cases elements of several models may be involved in a single eruption. While there is good evidence that magnetic flux ropes represent a preferred eruption topology, the manner of their formation for particular events—emergence from below the photosphere, in the corona prior to the eruption or in the later stages of the eruption itself, remains uncertain.

Availability of near-Earth (SOHO, ACE, WIND, Cluster, STEREO) and interplanetary (Ulysses) missions equipped with magnetometers, plasma and particle energy and composition analyzers has allowed the intensive study of the interplanetary consequences of solar eruptions (ICMEs) and of the more tightly defined entities known as Magnetic Clouds (MCs). In many cases a particular event has been registered as it encountered a single near-Earth spacecraft. This requires that a model of the cloud magnetic structure be fit to the data so that the associated magnetic flux and helicity may be deduced. This is done with reasonable reliability except in cases where the spacecraft to cloud impact parameter is large. However the quality of observations is much enhanced when a single structure is observed in-situ with multiple spacecraft. The availability of missions deploying several spacecraft e.g. Cluster, Double Star, STEREO, is making this increasingly possible. Comparisons of the cloud magnetic properties with those of the original erupting material can provide valuable insight into the original process though the situation is complicated by possible magnetic interactions by the cloud during its passage through the solar atmosphere to the in-situ spacecraft. Estimates of cloud transit speed can help to provide verification for associating a particular cloud with its original eruption which will typically have occurred two days earlier. In-situ composition measurements provide another useful basis for comparison between the cloud and the parent eruption and can help in understanding the origins of the latter. Here again interactions of the expanding shock with material in the solar atmosphere can complicate the picture. There is a growing realization that relating in-situ observations to remotely sensed views of the eruption site is valuable for understanding the interaction of solar eruptions with the near-Earth environment. This area, often described by the term "space weather", is assuming increased importance given the possibility that Sun–Earth interactions can result in damage to near-Earth space assets in general and to astronauts outside the Earth's magnetosphere in particular.

While much valuable work has been done by considering the properties of large numbers of events on a statistical basis, ultimate understanding of the physics involved, both at the Sun and in the interplanetary environment requires the detailed examination of individual eruptions both at the Sun and in the near-Earth environment. The complexities involved render this approach a difficult one as the examples addressed in Sect. 7 of this review have demonstrated. The existence of several possible mechanisms that give rise to eruptions at

the Sun presents particular challenges, especially in the case of large events where much of the solar atmosphere may be involved. As the history of solar flare studies has shown there is a danger that preoccupation with individual cases, both at the Sun and near the Earth, can obscure important features of events at both locations. Thus it is essential that as far as possible a common and broadly based approach is pursued for studies at both locations and in the interplanetary medium.

Acknowledgements We thank Kimberley Steed, MSSL Solar and Plasma Groups, for making available Fig. 8 in the paper. LvDG acknowledges Hungarian government grant OTKA T048961. JLC acknowledges the Leverhulme Trust for the award of an Emeritus Fellowship. We are also grateful for the help of the referee who suggested significant improvements to the paper.

References

W.P. Abbett, G.H. Fisher, Y. Fan, Astrophys. J. **546**, 1194–1203 (2001)
J.J. Aly, Astrophys. J. **283**, 349–362 (1984)
J.J. Aly, Astrophys. J. Lett. **375**, L61–L64 (1991)
M.D. Andrews, Sol. Phys. **218**, 261–279 (2003)
S.K. Antiochos, C.R. Devore, J.A. Klimchuk, Astrophys. J. **510**, 485–493 (1999)
G. Attrill, M.S. Nakwacki, L.K. Harra, L. van Driel-Gesztelyi, C.H. Mandrini, S. Dasso, J. Wang, Sol. Phys. **238**, 117–139 (2006)
G.D.R. Attrill, L.K. Harra, L. van Driel-Gesztelyi, P. Démoulin, Astrophys. J. **656**, L101–L104 (2007)
G. Barnes, K.D. Leka, Astrophys. J. **646**, 1303–1318 (2006)
G. Barnes, D.W. Longcope, K.D. Leka, Astrophys. J. **629**, 561–571 (2005)
M.A. Berger, Geophys. Astrophys. Fluid Dyn. **30**, 79–104 (1984)
A. Bleybel, T. Amari, L. van Driel-Gesztelyi, K.D. Leka, Astron. Astrophys. **395**, 685–695 (2002)
V. Bothmer, R. Schwenn, Ann. Geophys. **16**, 1–24 (1998)
A. Brandenburg, K. Subramanian, Phys. Rep. **417**, 1–4 (2005)
M.P. Brouwer, C. Zwaan, Sol. Phys. **129**, 221–246 (1990)
G.E. Brueckner et al., Sol. Phys. **162**, 357–402 (1995)
L.F. Burlaga et al., J. Geophys. Res. **10**, 277–295 (1998)
L. Burlaga, E. Sittler, F. Mariani, R. Schwenn, J. Geophys. Res. **86**, 6673–6684 (1981)
P. Caligari, F. Moreno-Insertis, M. Schüssler, Astrophys. J. **441**, 886–902 (1995)
R.C. Canfield, H.S. Hudson, D.E. McKenzie, Geophys. Res. Lett. **26**, 627–630 (1999)
R.C. Carrington, Mon. Not. R. Astron. Soc. **19**, 1–3 (1858)
J. Chae, Astrophys. J. **560**, L95–L98 (2001)
J. Chae, Y.-J. Moon, Y.D. Park, Sol. Phys. **223**, 39–55 (2004)
J. Chen, Astrophys. J. **338**, 453–470 (1989)
W.-Z. Chen, C. Liu, H. Song, N. Deng, C.-Y. Tan, H. Wang, Chin. J. Astron. Astrophys. **7**(5), 733–742 (2007)
M. Cheung, M. Schüssler, F. Moreno-Insertis, in *Chromospheric and Coronal Magnetic Fields*, ed. by D.E. Innes, A. Lagg, S.A. Solanki. ESA SP, vol. 596 (2005), pp. 541–545
Y. Cui, R. Li, L. Zhang, Y. He, H. Wang, Sol. Phys. **237**, 45–59 (2006)
Y. Cui, R. Li, H. Wang, H. He, Sol. Phys. **242**, 1–8 (2007)
A. Dal Lago et al., Sol. Phys. **222**, 323–328 (2004)
S. Dasso, C.H. Mandrini, P. Démoulin, C.J. Farrugia, J. Geophys. Res. **108**, 1362–1369 (2003)
S. Dasso, C.H. Mandrini, P. Démoulin, M.L. Luoni, A.M. Gulisano, Adv. Space Res. **35**, 711–724 (2005)
S. Dasso, C.H. Mandrini, P. Démoulin, M.L. Luoni, Astron. Astrophys. **455**, 349–359 (2006)
J.-P. Delaboudinière et al., Sol. Phys. **162**, 291–312 (1995)
P. Démoulin, Adv. Space Res. **39**, 1674–1693 (2007)
P. Démoulin, Ann. Geophys. **26**, 3113–3125 (2008)
P. Démoulin, M.A. Berger, Sol. Phys. **215**, 203–215 (2003)
P. Démoulin, E. Pariat, Adv. Space Res. (2008, in press)
P. Démoulin, C.H. Mandrini, L. van Driel-Gesztelyi, B.J. Thompson, S. Plunkett, Zs. Kövári, G. Aulanier, A. Young, Astron. Astrophys. **382**, 650–665 (2002)
N. Deng, Y. Xu, G. Yang, W. Cao, C. Liu et al., Astrophys. J. **644**, 1278–1291 (2006)
M. Dikpati, P.A. Gilman, Astrophys. J. **635**, L193–L196 (2005)
M. Dryer, Space Sci. Rev. **33**, 233–275 (1982)
M. Dryer et al., Sol. Phys. **181**, 159–183 (1998)

D.A. Falconer, J. Geophys. Res. **106**, 25185–25190 (2001)
D.A. Falconer, R.L. Moore, G.A. Gary, Astrophys. J. **569**, 1016–1025 (2002)
D.A. Falconer, R.L. Moore, G.A. Gary, J. Geophys. Res. **108**, 1380 (2003). CiteID 1380
D.A. Falconer, R.L. Moore, G.A. Gary, Astrophys. J. **644**, 1258–1272 (2006)
Y. Fan, Astrophys. J. **630**, 543–551 (2005)
Y. Fan, Astrophys. J. **676**, 680–697 (2008)
Y. Fan, G.H. Fisher, E.E. DeLuca, Astrophys. J. **405**, 390–401 (1993)
G.H. Fisher, Y. Fan, R.F. Howard, Astrophys. J. **438**, 463–471 (1995)
T.G. Forbes, J. Geophys. Res. **105**, 23153–23166 (2000)
T.G. Forbes, P.A. Isenberg, Astrophys. J. **373**, 294–307 (1991)
T.G. Forbes, E.R. Priest, P.A. Isenberg, Sol. Phys. **150**, 245–266 (1994)
M.K. Georgoulis, Geophys. Res. Lett. **35**, 6 (2008). CiteID L06S02
M.K. Georgoulis, B.J. LaBonte, Astrophys. J. **671**, 1034–1050 (2007)
M.K. Georgoulis, D.M. Rust, Astrophys. J. **661**, L109–L112 (2007)
S.E. Gibson, Y. Fan, J. Geophys. Res. **113**, A09103 (2008)
P.A. Gilman, Astron. Nachr. **326**, 208–217 (2005)
P.A. Gilman, M. Dikpati, Astrophys. J. **528**, 552–572 (2000)
A. Glover, L.K. Harra, S.A. Matthews, K. Hori, J.L. Culhane, Astron. Astrophys. **378**, 239–246 (2001)
G. Gloeckler et al., Geophys. Res. Lett. **26**, 157–160 (1999)
J.T. Gosling, V. Pizzo, S.J. Bame, J. Geophys. Res. **78**, 2001–2009 (1973)
J.T. Gosling, J.R. Asbridge, S.J. Bame, W.C. Feldman, G. Paschmann, N. Sckopke, J. Gepohys. Res. **85**, 744–752 (1980)
L.M. Green, M.C. López-Fuentes, C.H. Mandrini, P. Démoulin, L. van Driel-Gesztelyi, J.L. Culhane, Sol. Phys. **208**, 43–68 (2002a)
L.M. Green, S.A. Matthews, L. van Driel-Gesztelyi, L.K. Harra, J.L. Culhane, Sol. Phys. **205**, 325 (2002b)
L.M. Green, B. Kliem, T. Török, L. van Driel-Gesztelyi, G.D.R. Attrill, Sol. Phys. **246**, 365–391 (2007)
H.J. Hagenaar, R.A. Shine, Astrophys. J. **635**, 659–669 (2005)
H.J. Hagenaar, C.J. Schrijver, A.M. Title, Astrophys. J. **584**, 1107–1119 (2003)
G.E. Hale, Astrophys. J. **28**, 315–343 (1908)
G.E. Hale, S.B. Nicholson, Astrophys. J. **62**, 270–300 (1925)
G.E. Hale, F. Ellerman, S.B. Nicholson, A.H. Joy, Astrophys. J. **49**, 153–178 (1919)
L. Harra, A. Sterling, Astrophys. J. **561**, L215–L218 (2001)
L. Harra et al., Sol. Phys. **244**, 95–114 (2007)
K.L. Harvey, PhD Thesis, University of Utrecht (1993)
K. Harvey, J. Harvey, Sol. Phys. **28**, 61–71 (1973)
K.L. Harvey, C. Zwaan, Sol. Phys. **148**, 85–118 (1993)
D.H. Hathaway, D.P. Choudhary, Sol. Phys. **250**, 269–278 (2008)
J. Hirshberg, D.S. Colburn, Planet. Space Sci. **17**, 1183–1206 (1969)
A.W. Hood, E.R. Priest, Geophys. Astrophys. Fluid Dyn. **17**, 297–318 (1981)
H.S. Hudson, L.W. Acton, S.L. Freeland, Astrophys. J. **470**, 629–635 (1996)
A.J. Hundhausen, H.E. Gilbert, S.J. Bame, Astrophys. J. **152**, L3–L7 (1968)
A.J. Hundhausen, in *The Many Faces of the Sun*, ed. by K.T. Strong, J.L.R. Saba, B.M. Haisch, J.T. Schmelz (Springer, New York, 1999), pp. 143–200
H. Jeong, J. Chae, Astrophys. J. **671**, 1022–1033 (2007)
L.W. Klein, L.F. Burlaga, J. Geophys. Res. **87**, 613–624 (1982)
B. Kliem, T. Török, Phys. Rev. Lett. **96**, 255002–255006 (2006)
J.A. Klimchuk, in *Space Weather*, ed. by P. Song, H.J. Singer, J.L. Siscoe (2001), pp. 143–157
B.J. LaBonte, M.K. Georgoulis, D.M. Rust, Astrophys. J. **671**, 955–963 (2007)
K.D. Leka, G. Barnes, Astrophys. J. **595**, 1277–1295 (2003a)
K.D. Leka, G. Barnes, Astrophys. J. **595**, 1296–1306 (2003b)
K.D. Leka, G. Barnes, Astrophys. J. **656**, 1173–1186 (2007)
K.D. Leka, R.C. Canfield, A.N. McClymont, L. van Driel-Gesztelyi, Astrophys. J. **462**, 547–560 (1996)
R.P. Lepping et al., J. Geophys. Res. **102**, 14049–14064 (1997)
S.T. Lepri, T.H. Zurbuchen, J. Geophys. Res. **109**, A01112–A01124 (2004)
S.T. Lepri, T.H. Zurbuchen, L.A. Fisk, I.G. Richardson, H.V. Cane, G. Gloeckler, J. Geophys. Res. **106**, 29231–29238 (2001)
J. Lin, T.G. Forbes, P.A. Isenberg, P. Démoulin, Sol. Phys. **150**, 245–266 (1998)
J.A. Linker, Z. Mikić, P. Riley, R. Lionello, D. Odstrcil, Phys. Plasmas **10**, 1971–1978 (2003)
B.W. Lites, K.D. Leka, A. Skumanich, V. Martínez Pillet, T. Shimizu, Astrophys. J. **460**, 1019–1026 (1996)
B. Lites, H. Socas-Navarro, M. Kubo, T.E. Berger, Z. Frank, R.A. Shine, T.D. Tarbell, A.M. Title, K. Ichimoto, Y. Katsukawa, S. Tsuneta, Y. Suematsu, T. Shimizu, S. Nagata, Publ. Astron. Soc. Jpn. **59**, S571–S576 (2007)

Y. Liu, Astrophys. J. **679**, L151–L154 (2008)
D.W. Longcope, A.R. Choudhuri, Sol. Phys. **205**, 63–92 (2002)
D.W. Longcope, G.H. Fisher, Astrophys. J. **458**, 380–390 (1996)
D.W. Longcope, G.H. Fisher, S. Arendt, Astrophys. J. **464**, 999–1011 (1996)
D.W. Longcope, M.G. Linton, A.A. Pevtsov, G.H. Fisher, I. Klapper, in *Magnetic Helicity in Space and Laboratory Plasmas*, ed. by M.R. Brown, R.C. Canfield, A.A. Pevtsov. Geophys. Monograph, vol. 111 (AGU, Washington, 1999), p. 93
M. López-Fuentes, P. Démoulin, C.H. Mandrini, L. van Driel-Gesztelyi, Astrophys. J. **544**, 540–549 (2000)
M. López-Fuentes, P. Démoulin, C.H. Mandrini, A.A. Pevtsov, L. van Driel-Gesztelyi, Astron. Astrophys. **397**, 305–318 (2003)
B.C. Low, Sol. Phys. **167**, 216–265 (1996)
B.C. Low, Geophys. Monograph. **99**, 39–48 (1997)
B.C. Low, in *Solar Wind Nine, Proceedings of the Ninth International Solar Wind Conference*, ed. by S.R. Habbal, R. Esser, J.V. Hollweg, P.A. Isenberg. AIP Conf. Proc., vol. 471 (1999), p. 109
B.C. Low, D.F. Smith, Astrophys. J. **410**, 412–415 (1993)
M.L. Luoni, C.H. Mandrini, S. Dasso, L. van Driel-Gesztelyi, P. Démoulin, Tracing magnetic helicity from the solar corona to the interplanetary space. J. Atmos. Sol.–Terr. Phys. **67**, 1734–1743 (2005)
R.M. MacQueen et al., Astrophys. J. **187**, L85–L89 (1974)
R.M. MacQueen et al., Sol. Phys. **65**, 91–107 (1980)
T. Magara, A model for dynamic evolution of emerging magnetic fields in the Sun. Astrophys. J. **605**, 480–492 (2004)
W. Manchester, T. Gombosi IV, D. DeZeeuw, Y. Fan, Eruption of a buoyantly emerging magnetic flux rope 2004. Astrophys. J. **610**, 588–596 (2004)
A.N. McClymont, G.H. Fisher, in *Solar System Plasma Physics*, ed. by J.H. Waite, Jr., J.L. Burch, R.L. Moore (1989), pp. 219–228
C.H. Mandrini, S. Pohjolainen, S. Dasso, L.M. Green, P. Démoulin, L. van Driel-Gesztelyi, C. Copperwheat, C. Foley, Astron. Astrophys. **434**, 725–740 (2005)
C.H. Mandrini, M.S. Nakwacki, G. Attrill, L. van Driel-Gesztelyi, P. Démoulin, S. Dasso, H. Elliott, Sol. Phys. **244**, 25–43 (2007)
P.K. Manoharan, Sol. Phys. **148**, 153–167 (1993)
P.K. Manoharan, M. Kojima, N. Gopalswamy, T. Kondo, Z. Smith, Astrophys. J. **530**, 1061–1070 (2000)
P.K. Manoharan, S. Ananthakrishnan, M. Dryer, T.R. Detman, H. Leinbach, M. Kojima, T. Watanabe, J. Kahn, Sol. Phys. **156**, 377–393 (1995)
S.F. Martin, S.H.B. Livi, J. Wang, Aust. J. Phys. **38**, 929–959 (1985)
K. Marubashi, in *Coronal Mass Ejections*, ed. by N. Crooker, J.A. Joselyn, J. Feynmann, AGU Geophys. Monograph, vol. 99 (1997), p. 147
D.B. Melrose, Astrophys. J. **387**, 403–413 (1992)
N. Meunier, Astron. Astrophys. **405**, 1107–1120 (2003)
G. Michałek, N. Gopalswamy, S. Yashiro, Astrophys. J. **584**, 472–478 (2003)
F. Moreno-Insertis, T. Emonet, Astrophys. J. **472**, L53–L56 (1996)
F. Moreno-Insertis, P. Caligari, M. Schüssler, Sol. Phys. **153**, 449–452 (1994)
G.E. Moreton, H.E. Ramsey, Publ. Astron. Soc. Pac. **72**, 357–359 (1960)
M.J. Murray, A.W. Hood, Astron. Astrophys. **479**, 567–577 (2008)
G. Newkirk, Astrophys. J. **133**, 983–1013 (1961)
A. Nindos, M.D. Andrews, Astrophys. J. **616**, L175–L178 (2004)
T.J. Okamoto et al., Astrophys. J. **673**, L215–L218 (2008)
E. Pariat, G. Aulanier, B. Schmieder, M.K. Georgoulis, D.M. Rust, P.N. Bernasconi, Astrophys. J. **614**, 1099–1112 (2004)
E. Pariat, P. Démoulin, M.A. Berger, Astron. Astrophys. **439**, 1191–1203 (2005)
E. Pariat, A. Nindos, P. Démoulin, M.A. Berger, Astron. Astrophys. **452**, 623–630 (2006)
E.N. Parker, Astrophys. J. **408**, 707–719 (1993)
A.A. Pevtsov, Astrophys. J. **531**, 553–560 (2000)
A.A. Pevtsov, K.S. Balasubramaniam, Adv. Space Res. **32**, 1867–1874 (2003)
A.A. Pevtsov, R.C. Canfield, S.M. Latushko, Astrophys. J. **549**, L261–L263 (2001)
S. Règnier, E.R. Priest, Astron. Astrophys. **468**, 701–709 (2007)
I.G. Richardson, in *Coronal Mass Ejections*, ed. by N. Crooker, J.A. Joselyn, J. Feynmann, AGU Geophys. Monograph, vol. 99 (1997), p. 189
I.G. Richardson, H.V. Cane, J. Geophys. Res. **109**, A09104–A09120 (2004)
I.G. Richardson, H.V. Cane, T.T. von Rosenvinge, J. Geophys. Res. **96**, 7853–7860 (1991)
D.M. Rust, Geophys. Res. Lett. **21**, 241–244 (1994)
D.M. Rust, A. Kumar, Astrophys. J. Lett. **464**, L199–L203 (1996)

D.M. Rust, B.J. Anderson, M.D. Andrews, M.H. Acuña, C.T. Russell, P.W. Schuck, T. Mulligan, Astrophys. J. **621**, 524–536 (2005)
M. Ryutova, H. Hagenaar, Sol. Phys. **246**, 281–294 (2007)
A. Sainz Dalda, V. Martínez Pillet, Astrophys. J. **632**, 1176–1183 (2005)
K. Saito, Ann. Tokyo Astron. Obs. **12**, 53–120 (1970)
H.U. Schmidt, in *Structure and Development of Solar Active Regions*, ed. by K.O. Keipenheuer. IAU Symp., vol. 35 (1968), pp. 95–107
C.J. Schrijver, Astrophys. J. **655**, L117–L120 (2007)
C.J. Schrijver, C. Zwaan, *Solar and Stellar Magnetic Activity*. Cambridge Astrophysics Series, vol. 34 (Cambridge University Press, New York, 2000)
C.J. Schrijver, M.L. DeRosa, A.M. Title, T.R. Metcalf, Astrophys. J. **628**, 501–513 (2005)
C.J. Schrijver, M.L. DeRosa, T. Metcalf, G. Barnes, B. Lites et al., Astrophys. J. **675**, 1637–1644 (2008)
M. Schüssler, Astron. Astrophys. **71**, 79–91 (1979)
R. Schwenn, A. Dal Lago, E. Huttunen, W.D. Gonzalez, Ann. Geophys. **23**, 1033–1059 (2005)
A. Sterling, H.S. Hudson, Astrophys. J. Lett. **491**, L55–L59 (1997)
P.A. Sturrock, Astrophys. J. **380**, 655–659 (1991)
J.J. Sudol, J.W. Harvey, Astrophys. J. **635**, 647–658 (2005)
S.J. Tappin, Planet. Space Sci. **34**, 93–97 (1986)
B.J. Thompson, S.P. Plunkett, J.B. Gurman, J.S. Newmark, O.C. StCyr, D.J. Michels, Geophys. Res. Lett. **25**, 2465–2468 (1998)
L. Tian, D. Alexander, Astrophys. J. **673**, 532–543 (2008)
V.S. Titov, P. Démoulin, Astron. Astrophys. **351**, 707–720 (1999)
T. Török, B. Kliem, Astrophys. J. **630**, L97–L100 (2005)
T. Török, B. Kliem, Astron. Nachr. **328**, 743–746 (2007)
T. Török, B. Kliem, V.S. Titov, Astron. Astrophys. **413**, L27–L30 (2004)
D. Tripathi, S.E. Gibson, J. Qiu, L. Fletcher, R. Liu, H. Gilbert, H.E. Mason, Astron. Astrophys. (2008, submitted)
S. Tsuneta et al., Sol. Phys. **249**, 167–196 (2008)
A.A. van Ballegooijen, P.C.H. Martens, Astrophys. J. **343**, 971–984 (1989)
L. van Driel-Gesztelyi, in *Three-Dimensional Structure of Solar Active Regions*, ed. by C.E. Alissandrakis, B. Schmieder. ASP Conf. Ser., vol. 155 (1998), pp. 202–223
L. van Driel-Gesztelyi, K. Petrovay, Sol. Phys. **126**, 285–298 (1990)
L. van Driel-Gesztelyi, C.H. Mandrini, B. Thompson, S. Plunkett, G. Aulanier, P. Démoulin, B. Schmieder, C. de Forest, in *Third Advances in Solar Physics Euroconference: Magnetic Fields and Oscillations*, ed. by B. Schmieder, A. Hofmann, J. Staude, vol. 184 (1999), pp. 302–306
L. van Driel-Gesztelyi, P. Démoulin, C.H. Mandrini, L. Harra, J.A. Klimchuk, Astrophys. J. **586**, 579–591 (2003)
B. Vršnak, J. Magdalenić, P. Zlobec, Astron. Astrophys. **413**, 753–763 (2004)
J. Wang, Sol. Phys. **163**, 319–325 (1996)
H. Wang, H. Zirin, G. Ai, Sol. Phys. **131**, 53–68 (1991)
H. Wang, H. Sung, J. Jing, V. Yurchishyn, Y.-Y. Deng, H.-Q. Zhang, D. Falconer, J. Li, Chin. J. Astron. Astrophys. **6**, 477–488 (2006)
D.F. Webb et al., J. Geophys. Res. **105**, 27251–27260 (2000)
J.P. Wild, L.L. McCready, Aust. J. Sci. Res. A **3**, 387–398 (1950)
J.P. Wild, S.F. Smerd, Ann. Rev. Astron. Astrophys. **10**, 159–156 (1972)
D.R. Williams, T. Török, P. Démoulin, L. van Driel-Gesztelyi, B. Kliem, Astrophys. J. **628**, L163–L166 (2005)
R. Wolfson, S. Saran, Astrophys. J. **499**, 496–503 (1998)
S.T. Wu, Space Sci. Rev. **32**, 115–129 (1982)
P. Wurz, P. Bochsler, M.A. Lee, J. Geophys. Res. **105**, 27239–27250 (2000)
M. Zhang, B.C. Low, Ann. Rev. Astron. Astrophys. **43**, 103–137 (2005)
X.P. Zhao, J.T. Hoeksema, J. Geophys. Res. **103**, 2077–2083 (1998)
T.H. Zurbuchen, I.G. Richardson, Space Sci. Rev. **123**, 31–43 (2006)